PROCEEDINGS A

royalsocietypublishing.org/journal/rspa

Research

Cite this article: Breunung T. 2022 Asymptotic stability of quasi-periodic orbits. *Proc. R. Soc. A* **478**: 20210787. https://doi.org/10.1098/rspa.2021.0787

Received: 8 October 2021
Accepted: 14 February 2022

Subject Areas:
mechanical engineering, applied mathematics, differential equations

Keywords:
vibrations, nonlinear oscillations, stability, quasi-periodic oscillations, computational algorithm, linear time-varying systems

Author for correspondence:
Thomas Breunung
e-mail: thomasbr@umd.edu

†Present address: Department of Mechanical Engineering, University of Maryland, College Park, MD 20742, USA.

Asymptotic stability of quasi-periodic orbits

Thomas Breunung

Institute for Mechanical Systems, ETH Zürich, Leonardstrasse 21, Zürich 8092, Switzerland

TB, 0000-0001-7885-2201

Stability is one of the most fundamental properties of solutions to differential equations and, for example, can explain the presence of harmful vibrations. While the stability type of fixed points and periodic orbits can be assessed with standard tools, no general and reliable method allows to conclude about the stability of quasi-periodic orbits. Here, we overcome this limitation and develop a novel and universal method to rigorously assess the asymptotic stability of quasi-periodic solutions to differential equations. Furthermore, we develop an automated algorithm for such stability investigations and demonstrate its applicability on two explicit mechanical examples.

1. Introduction

It is of vital importance to assess the stability of computed solutions to differential equations modelling physical processes since their long-term behaviour is governed by stable solutions. Such solutions include quasi-periodic orbits, which have been observed in the cochlea excited through sound waves (e.g. Karavitaki & Mountain [1]), oxidation reactions (cf. Hauck & Schneider [2]) and in many classical engineering applications such as brake squeal (cf. Oberst & Lai [3]), fluid flows (cf. Walden *et al.* [4]) and electric circuits (cf. Cumming & Linsay [5]). Moreover, analyses dating back to the work of Laplace and Lagrange show that the motions of our solar system's planets are quasi-periodic at first order (Laskar [6]). While many computational tools (e.g. Chua & Ushida [7], Dieci *et al.* [8] or Schilder *et al.* [9]) succeed to compute quasi-periodic solutions to differential equations, their stability, however, remains generally unclear.

The stability type of quasi-periodic solutions has been assessed with direct numerical time integration. We refer to Zounes & Rand [10] or the review by Kovacic *et al.* [11] for stability investigations of the Mathieu equation with a quasi-periodic stiffness term. For some initial

THE ROYAL SOCIETY PUBLISHING

time and initial conditions, the equations of variation are integrated and then the observed decay or growths is linked to stability. The classical definition of asymptotic stability (cf. Verhulst [12] or definition A.1 of appendix A), however, requires the knowledge of solutions for all initial times and all initial conditions in a neighbourhood of the quasi-periodic solution for arbitrarily large time intervals, i.e. an infinite number of integrated trajectories for infinite time spans. This task is infeasible for a computer. Hence, the relevance of a selected number of trajectories over a finite time span for asymptotic stability of quasi-periodic orbits is not immediate.

In the periodic case, linearizing along the periodic orbit yields the linear time-periodic equations of variation. Thus, the eigenvalues of the monodromy matrix allow to conclude about their stability type (e.g. Verhulst [12] or Teschl [13]). In this context, a theorem by Floquet guarantees that the linear and time-periodic equations of variation can be transformed into a linear system with constant coefficients. In the more general quasi-periodic case systems with such a transformation, i.e. transforming the linear time-varying linearization into a linear system with constant coefficients, are referred to as reducible. With such an envisioned transformation at hand, stability investigations reduce to eigenvalue computations of a matrix with constant coefficients. However, only special systems are known to be reducible. For example, if the time-varying linearization has a point spectrum, then a result by Johnson & Sell [14] can guarantee reducibility. However, to the best of our knowledge, it is generally unclear if a given quasi-periodic linearization possesses a point spectrum. Alternatively, if the time-varying terms are small, then a result by Jorba & Simó [15] can guarantee the reducibility of the quasi-periodic linearization. In the general case, however, it is unfortunately unclear whether a given quasi-periodic linearization is reducible.

Even if a linear quasi-periodic system is reducible, then the transformed system with constant coefficients or at least its eigenvalues need to be computed. To this end, Jorba [16] proposes a numerical algorithm by solving a generalized eigenvalue problem. Selecting several Poincare sections, the arising non-autonomous Poincare map for each section is discretized via a truncated Fourier series. Thereby, the generalized eigenvalue problem is approximated by a finite-dimensional operator. Expanding the same generalized eigenvalues problem in Fourier space, i.e. without introducing a Poincare section, one obtains a method referred to as Hill's method (cf. Lazarus & Thomas [17]). However, as Jorba [16] admits, the eigenvalues of the discretized eigenvalue problem do not necessarily correspond to the eigenvalues of the generalized eigenvalue problem. Hence, stability conclusions based on the discretized operator are questionable. Already for periodic systems, there are examples where an application of Hill's method leads to wrong conclusions (cf. Krack & Gross [18]). Furthermore, the discretized operator is a large matrix and computation of its eigenvalues can lead to a significant computational burden (cf. Peletan *et al.* [19] for an example from rotor dynamics).

Another strategy to assess the stability of quasi-periodic orbits with readily available results from the periodic case was proposed by Zounes & Rand [10] or Sharma & Sinha [20] considering the Mathieu equation with quasi-periodic time dependence and Guskov & Thouverez [21] investigating a quasi-periodically driven Duffing oscillator. They approximate the incommensurate frequency basis of the quasi-periodic orbit with a rational related one. Indeed, every irrational fraction can be arbitrarily well approximated by integer fractions. The arising system is periodic and hence stability analysis can be carried out via numerical computation of the monodromy matrix. Unfortunately, the connection between the stability type of the periodic approximation to the stability type of the quasi-periodic linearization remains unclear.

If the quasi-periodic orbit of interest is close to another orbit with known stability type, then its stability can be accessed with perturbation methods such as the method of averaging (cf. Sanders *et al.* [22]), the method of multiple time scales (cf. Nayfeh [23]) or normal forms (cf. Murdock [24]). For example, Belhaq & Houssni [25] apply the method of averaging and then subsequently a multiple time scales argument to assess the stability of a Duffing oscillator with parametric and external excitation. Furthermore, Guennoun *et al.* [26] apply the method of multiple time scales twice to investigate the stability of a Mathieu equation with quasi-periodic parametric excitation. We also refer to Zounes & Rand [10] for a specific perturbation method to obtain curves

separating stable and unstable parameter regions of the Mathieu equation with quasi-periodic parametric excitation. Moreover, results on the persistence of invariant tori by Samoilenko [27] or Haro & de la Llave [28] can guarantee that the stability of the quasi-periodic orbit is preserved for small enough perturbations. Besides applying to specific systems only, the main drawback of such perturbation approaches is their generally unknown domain of validity. It is restricted to a small neighbourhood of the unperturbed limit. Whether the orbit of interest is contained within this neighbourhood is generally unclear.

Technically, computing the largest Lyapunov exponent along a quasi-periodic orbit (cf. Oseledec [29] or Pesin [30]) reveals the stability type of this solution. In a series of papers Benettin *et al.* [31–33] subsequently develop an algorithm to compute the Lyapunov spectrum relying on frequent renormalization and reorthogonalization. Moreover, Wolf *et al.* [34] propose a method to compute Lyapunov exponents from a single time series. We also refer to Skokos [35] and Pikovsky & Politi [36] for detailed remarks on Lyapunov exponents and their computation. Additionally, the generalized Lyapunov type number introduced by Fenichel [37] can also be related to stability. However, all these exponents are asymptotic quantities, i.e. they are defined in the limit as the time approaches infinity. This limit cannot be realized on a computer (see also a remark by Wiggins [38]). Indeed, Dieci *et al.* [39] admit that determining a suitable truncation time is nontrivial. Moreover, Benettin *et al.* [32] point out that numerical errors can accumulate over the long integration times necessary to observe these asymptotic quantities.

Noticing the difficulties encountered when computing the largest Lyapunov exponent, alternative indicators have been suggested to conclude about the sign of the largest Lyapunov exponent. For example, Froeschlé *et al.* [40] and Froeschlé & Lega [41] propose a series of fast Lyapunov indicators, which they use to study a series of dynamical systems arising in celestial mechanics. Moreover, Skokos [42] proposes an alignment index which has been subsequently generalized by Skokos *et al.* [43] to capture more details about the geometry of the investigated orbit. The aforementioned indicators show a trend as time goes to infinity from which one then can conclude about the sign of the largest Lyapunov exponent. While these indicators can be more efficient than computing the largest Lyapunov exponent (e.g. Manos *et al.* [44]), the fundamental issue, i.e. the necessity to observe a trend as time goes to infinity, remains. In practice, these computations are truncated at some finite time and it is generally unclear whether the observed behaviour of an indicator is its asymptotic trend or a transient phenomenon.

Normal infinitesimal Lyapunov exponents (NILEs) defined by Haller & Sapsis [45], by contrast, are instantaneous quantities, i.e. do not require an infinite time horizon as the Lyapunov exponents. NILEs characterize instantaneous growth or decay of perturbations initiated into the normal space of a manifold. If all the NILEs along the closure of a quasi-periodic solution indicate an instantaneous decay, then the torus attracts nearby solutions and is exponentially stable. This condition, however, is restrictive as it does not allow for any localized (in time or space) repulsion of trajectories.

In a series of papers, Kaas-Petersen [46–48] introduces a new type of Poincare return map to compute quasi-periodic orbits and assess their stability type. He relies on the fact, that quasi-periodic orbits can be described by introducing phases defined on the standard torus of appropriate dimension. The time evolution of these phases is dense on the torus. Thus, starting from some initial phases, there will be infinitely many time instances such the phases are arbitrarily close to their initial values. Selecting an appropriate set of such time instances, Kaas–Petersen interpolates a return map for a time span such that the phases have exactly returned to their initial values. By definition of quasi-periodicity, however, such an envisioned time does not exist and hence the relevance of the interpolated mapping for the dynamical system is unclear. Furthermore, the error due to interpolation remains unknown and as Schilder *et al.* [9] note the algorithm suffers from a small divisor problem.

In summary, the numerical methods assessing stability of quasi-periodic orbits rely on heuristic assumptions and lack a rigorous basis, while perturbation arguments are restricted to specific systems and their domain of validity is generally unclear. Here, we propose a rigorous and versatile method to assess whether a quasi-periodic orbit is asymptotically stable. Asymptotic

stability (cf. appendix A definition A.1) is a fundamental characteristic of solutions to dissipative systems. Similar to the periodic case (cf. Guckenheimer & Holmes [49]), our argument relies on an iterated map. Discretizing this map over the torus appropriately and establishing an explicit robustness estimate, we show that based on a finite number of trajectories integrated over a finite time, we can conclude about asymptotic stability of a quasi-periodic orbit. Moreover, we provide an explicit numerical implementation of our algorithm[1] and demonstrate its application to two mechanical systems.

2. Set-up

We consider the linearization of a dynamical system along a quasi-periodic orbit given by

$$\dot{\mathbf{x}} = \mathbf{A}(\Omega_1 t, \Omega_2 t, \ldots, \Omega_K t)\mathbf{x} \quad \text{and} \quad \mathbf{x}(t_0) = \mathbf{x}_0, \quad \mathbf{x} \in \mathbb{R}^N, \tag{2.1}$$

where the matrix $\mathbf{A}(\phi_1, \phi_2, \ldots, \phi_k)$ is 2π periodic and continuously differentiable in its arguments. Its arguments ϕ_k are denoted as phases. Due to the periodicity each phase ϕ_k can be restricted to take values between 0 and 2π. Hence, the domain of the vector $\boldsymbol{\phi}$ is the K-dimensional torus $\mathbb{T}^K = (\mathbb{R}/(2\pi))^K := [0, 2\pi) \times [0, 2\pi) \times \cdots \times [0, 2\pi)$. The initial condition is denoted by $\mathbf{x}_0$.

We collect the external forcing frequencies Ω_k in the vector $\boldsymbol{\Omega} := [\Omega_1, \Omega_2, \ldots, \Omega_K]$. Without loss of generality, we assume that $\boldsymbol{\Omega}$ is incommensurate, i.e.

$$\langle \boldsymbol{\kappa}, \boldsymbol{\Omega} \rangle = \sum_{k=1}^{K} \kappa_k \Omega_k \neq 0, \quad \text{for all } \boldsymbol{\kappa} \in \mathbb{Z}^K - \{\mathbf{0}\}, \tag{2.2}$$

holds. For the periodic case ($K = 1$), the stability of the origin of system (2.1) can be assessed through the eigenvalues of principal matrix solution at the time $T = 2\pi/\Omega_1$. The underlying argument is either based a theorem by Floquet (e.g. Teschl [13] or Verhulst [12]) or the Poincare return map (e.g. Guckenheimer & Holmes [49]). These arguments, however, do not extend to the quasi-periodic case ($K > 1$).

To numerically check whether the origin of system (2.1) is asymptotically stable (cf. definition A.1 in appendix A) one faces two challenges. First, asymptotic stability requires the knowledge of trajectories as time approaches infinity, which cannot be observed numerically without additional arguments. Furthermore, for asymptotic stability, trajectories need to decay for all initial times t_0, i.e. infinitely many initial time instances. Again, this cannot be observed numerically, since only an invariably finite number of numerical computations can be carried out. To overcome the two aforementioned challenges, we rely on the fact that the phases $\boldsymbol{\phi}(t)$ evolve inside the compact K-dimensional torus $\mathbb{T}^K$.

3. Asymptotic stability of linear quasi-periodic systems

Asymptotic stability (cf. definition A.1) requires the solutions of the initial value problem of equation (2.1). For each time instance t, the phases $\boldsymbol{\phi}(t)$ take values $\boldsymbol{\phi}(t) \in \mathbb{T}^K$. We denote the initial angle by $\boldsymbol{\phi}(t_0) = \boldsymbol{\phi}_0$, the difference between the time t and the initial time by τ (i.e. $\tau = t - t_0$) and rewrite the initial value problem of equation (2.1) as

$$\frac{\mathrm{d}}{\mathrm{d}\tau}\mathbf{x} = \dot{\mathbf{x}} = \mathbf{A}(\boldsymbol{\Omega}(\tau + t_0))\mathbf{x} = \mathbf{A}(\boldsymbol{\Omega}\tau + \boldsymbol{\phi}_0)\mathbf{x} \quad \text{and} \quad \mathbf{x}(\tau = 0) = \mathbf{x}(t_0) = \mathbf{x}_0. \tag{3.1}$$

For system (3.1), we introduce the solution map mapping initial conditions $\mathbf{x}_0$ at the initial angle $\boldsymbol{\phi}_0$ to their later position at time τ, i.e.

$$\Pi^\tau(\boldsymbol{\phi}_0) \colon \mathbb{R}^N \to \mathbb{R}^N \quad \text{and} \quad \mathbf{x}(\tau) = \Pi^\tau(\boldsymbol{\phi}_0)\mathbf{x}_0. \tag{3.2}$$

The solution map $\Pi^\tau(\boldsymbol{\phi}_0)$ is similar to the well-known principal solution matrix $\Pi^t_{t_0}$ mapping initial conditions $\mathbf{x}_0$ at the time instance $t = t_0$ initial conditions $\mathbf{x}_0$ to their later position at time

[1]The automated MATLAB script QPSTAB is publicly available at github.com/tbreunung/QPstab.

t (cf. Teschl [13]). The main difference is the domain of the initial time t_0 of $\Pi_{t_0}^t$ compared with dependence of $\Pi^\tau(\boldsymbol{\phi}_0)$ on the initial angle $\boldsymbol{\phi}_0$. While the domain of the initial angle $\boldsymbol{\phi}_0$ is the compact K-dimensional torus, the initial time t_0 for the principal matrix solution $\Pi_{t_0}^t$ takes values from the non-compact real line.

The map (3.2) can be obtained by solving (e.g. numerically) equation (3.1) for finite times. Since the map $\Pi^\tau(\boldsymbol{\phi}_0)$ is prominent in our investigations, we clarify its meaning by relating $\Pi^\tau(\boldsymbol{\phi}_0)$ to the normal spaces of the autonomous system equivalent to equation (2.1).

(a) The map $\Pi^\tau(\boldsymbol{\phi}_0)$ and the normal spaces of the associated autonomous system

The autonomous equivalent to system (2.1) given by

$$\frac{\mathrm{d}}{\mathrm{d}t}\begin{bmatrix}\boldsymbol{x}\\ \boldsymbol{\phi}\end{bmatrix}=\begin{bmatrix}\mathbf{A}(\boldsymbol{\phi})\boldsymbol{x}\\ \boldsymbol{\Omega}\end{bmatrix}\quad\text{and}\quad \mathbf{y}:=[\boldsymbol{x},\boldsymbol{\phi}]\in\mathbb{R}^N\times\mathbb{T}^K=:\mathbb{P}, \tag{3.3}$$

where $\mathbb{P}$ denotes the phase space of system (3.3). Then, $\mathcal{M}:=\mathbf{0}\times\mathbb{T}^K$ is an invariant manifold for system (3.3). The vectors in the normal space $N_{\mathbf{y}}\mathcal{M}$ for any phase space location $\mathbf{y}\in\mathcal{M}$ point along the $\mathbf{x}$-coordinates only. Thus, the orthogonal projection of any vector $\mathbf{v}$ based at $\mathbf{y}$ into the normal space $N_{\mathbf{y}}\mathcal{M}$ is given by

$$\Pi_{N_{\mathbf{y}}\mathcal{M}}=\begin{bmatrix}\mathbf{I}_N & \mathbf{0}\\ \mathbf{0} & \mathbf{0}\end{bmatrix}\in\mathbb{R}^{(N+K)\times(N+K)},\quad\text{for all }\mathbf{y}\in\mathcal{M}, \tag{3.4}$$

where $\mathbf{I}_N$ denotes the identity matrix in $\mathbb{R}^{N\times N}$. We denote the linearized flow map of the autonomous dynamical system (3.3) by $\mathbf{DF}^t(\mathbf{y}_0)$. Following Fenichel [37], we define the mapping between normal spaces

$$\left.\begin{aligned}&\mathbf{N}^t(\mathbf{y}_0):N_{\mathbf{y}_0}\to N_{\mathbf{y}(t)},\\ &\mathbf{n}_t=\Pi_{N_{\mathbf{y}(t)}}\mathbf{DF}^t(\mathbf{y}_0)\mathbf{n}_0=\begin{bmatrix}\mathbf{I}_N & \mathbf{0}\\ \mathbf{0} & \mathbf{0}\end{bmatrix}\mathbf{DF}^t(\mathbf{y}_0)\begin{bmatrix}\mathbf{x}_0\\ \mathbf{0}\end{bmatrix}=\begin{bmatrix}\Pi^t(\boldsymbol{\phi}_0)\mathbf{x}_0\\ \mathbf{0}\end{bmatrix},\end{aligned}\right\}$$

which shows that the mapping (3.2) maps normal spaces along the invariant manifold $\mathcal{M}\in\mathbb{P}$ of autonomous system (3.3). Thus, it reveals whether the perturbation $\mathbf{x}_0$ into the normal space $N_{\mathbf{y}}$ increases or decreases in time.

Remark 3.1 (Autonomous dynamical systems). In some applications, quasi-periodic motions occur when an autonomous dynamical system is confined to a K-dimensional torus. If the linearization along this torus can be written in the canonical form (3.3), then the developed techniques can be applied to investigate normal stability of the torus, i.e. stability with respect to perturbations into the normal space.

After providing a geometric picture of the map $\Pi^\tau(\boldsymbol{\phi}_0)$, we assess its magnitude. To this end, we denote the square root of the maximal and the minimal eigenvalue of the symmetric matrix $\Pi^\tau(\boldsymbol{\phi}_0)(\Pi^\tau(\boldsymbol{\phi}_0))^\top$ by $\rho_{\max}$ and $\rho_{\min}$, i.e. we define

$$\rho_{\max}(\tau,\boldsymbol{\phi}_0):=\sqrt{\max[\mathrm{eig}[\Pi^\tau(\boldsymbol{\phi}_0)(\Pi^\tau(\boldsymbol{\phi}_0))^\top]]} \tag{3.5}$$

and

$$\rho_{\min}(\tau,\boldsymbol{\phi}_0):=\sqrt{\min[\mathrm{eig}[\Pi^\tau(\boldsymbol{\phi}_0)(\Pi^\tau(\boldsymbol{\phi}_0))^\top]]}. \tag{3.6}$$

The quantity $\rho_{\max}$ denotes the maximal growths or minimal decay of initial conditions of equation (3.1), while $\rho_{\min}$ denotes the minimal growths or maximal decay of initial conditions. Hence, if $\rho_{\max}(\tau,\boldsymbol{\phi}_0)$ is less than one for some τ and $\boldsymbol{\phi}_0$, then all initial conditions of system (3.1) decay for the specific angle $\boldsymbol{\phi}_0$ until the time τ. We would expect that if solutions to system (3.1) decay for all initial angles, then the origin of system (2.1) is asymptotically stable. To formulate this observation more precisely, we introduce the notation of a *contractive cover*:

Definition 3.2 (Contractive cover). The origin of system (2.1) has a *contractive cover*, if for all $\boldsymbol{\phi}_0 \in \mathbb{T}^K$, there exists some $T(\boldsymbol{\phi}_0) < \infty$ such that

$$\rho_{\max}(T(\boldsymbol{\phi}_0), \boldsymbol{\phi}_0) < 1, \tag{3.7}$$

holds.

The following result clarifies the relationship between asymptotic stability of the origin of system (2.1) and definition 3.2:

Theorem 3.3. *Definition* 3.2 *is equivalent to asymptotic stability of the origin of system* (*2.1*).

Proof. We detail the proof of the above theorem in appendix A. ∎

Compared to the classic definition of asymptotic stability, condition (3.7) does not require a limit for infinite times and hence can be point-wise verified.

Remark 3.4. If a contractive cover exists, then in appendix A, we prove that

$$\lim_{\tau \to \infty} ||\Pi^\tau(\boldsymbol{\phi}_0)|| = 0, \quad \text{for all } \boldsymbol{\phi}_0 \in \mathbb{T}^K, \tag{3.8}$$

holds. Together with equation (3.5), equation (3.8) shows that

$$\lim_{t \to \infty} \frac{|\mathbf{N}^t(\mathbf{y}_0)\mathbf{n}_0|}{|\mathbf{n}_0|} \to 0, \quad \forall\, \mathbf{y}_0 \in \mathcal{M},\ \mathbf{n}_0 \in N_{\mathbf{y}_0}\mathcal{M}, \tag{3.9}$$

holds. Hence, perturbations normal to the torus $\mathcal{M}$ in the extended phase space $\mathbb{P}$ decay asymptotically, which is the justification of Fenichel's interpretation of condition (3.9) as a stability condition. However, we note that condition (3.9) does generally not imply asymptotic stability of trajectories $\mathbf{y}(t; t_0, \mathbf{y}_0) \in \mathcal{M}$ in the extended phase space $\mathbb{P}$. The reason is that perturbations to the angle $\boldsymbol{\phi}_0$, i.e. perturbations inside the tangent space of $\mathcal{M}$, will not decay due to constant growth of the phases in equation (3.3).

Remark 3.5 (Finite-time Lyapunov exponents). Taking the logarithm of $\rho_{\max}$ and dividing it by τ yields the largest finite-time Lyapunov exponent (FTLE). FTLEs are a diagnostics to explore the phase space of general dynamical systems and are prominently applied in fluid dynamics (cf. Haller [50]). Our theorem 3.3 can be rephrased in terms of FTLEs. If for every initial angle, there exists a time instance such that the largest FTLE is negative, then the origin of system (2.1) is asymptotically stable.

Remark 3.6 (NILEs). Compared with a stability criterion from Haller & Sapsis [45] based on NILEs, we allow that trajectories of system (3.3) separate from $\mathcal{M} := \mathbf{0} \times \mathbb{T}^K$ for some times. We only require that for some time instance $T(\boldsymbol{\phi}_0)$ all normal perturbations are less than their initial value, which is less restrictive.

Remark 3.7 (Hamiltonian systems). Hamiltonian systems cannot feature an asymptotically stable origin and hence our developments do not apply to such systems. Indeed, Liouville's formula (e.g. Chicone [51]) implies that the determinant of the matrix $\Pi^\tau(\boldsymbol{\phi}_0)$ is one. Thus, the product of the eigenvalues of the matrix $\Pi^\tau(\boldsymbol{\phi}_0)(\Pi^\tau(\boldsymbol{\phi}_0))^\top$ is equal to one. Therefore, either the magnitude of all these eigenvalues is equal to one or at least one eigenvalue is greater than one in magnitude. Together, both cases imply $\rho_{\max} \geq 1$ (cf. equation (3.5)), which contradicts condition (3.7).

Condition (3.7) needs to hold for the K-dimensional torus. By introducing a Poincare section, i.e. fixing a phase and selecting the time T in definition 3.2 to be an integer multiple of one of the periods $T_j = 2\pi/\Omega_j$, we achieve a dimension reduction by one. Without loss of generality, we fix $\phi_1 = \phi_1^*$ and $T = 2\pi/\Omega_1$, introduce the reduced phase $\tilde{\boldsymbol{\phi}} \in \mathbb{T}^{K-1}$ and define a *contractive trap*:

Definition 3.8 (Contractive trap). There exists a *contractive trap* for the origin of system (2.1), if for some $\phi_1^* \in [0, 2\pi]$ and all $\tilde{\boldsymbol{\phi}}_0 \in \mathbb{T}^{K-1}$, there exists some integer $N = N(\phi_1^*, \tilde{\boldsymbol{\phi}}_0) < \infty$ such that

$$\rho_{\max}(NT, [\phi_1^*, \tilde{\boldsymbol{\phi}}_0]) < 1, \quad T := \frac{2\pi}{\Omega_1}, \tag{3.10}$$

holds.

We state the relationship between an contractive trap and asymptotic stability of the origin of system (2.1) in the following lemma:

Lemma 3.9. *Definition* 3.8 *is equivalent to asymptotic stability of the origin of system (2.1).*

Proof. In appendix B, we proof that the definitions 3.2 and 3.8 are equivalent for the origin of system (2.1). Then, by the virtue of theorem 3.3 the existence of a contractive trap is equivalent to asymptotic stability of the origin of system (2.1). ■

The main difference between conditions (3.7) and (3.10) is that condition (3.10) needs to be verified on a lower dimensional torus. Thus, to verify condition (3.10) numerically, we need to sample a lower dimensional torus compared with verification of condition (3.7).

Whether condition (3.7) or (3.10) are satisfied for some $\boldsymbol{\phi}_0$ can be verified e.g. numerically. However, definition 3.2 requires equation (3.7) to hold for all initial angles on the K-dimensional torus $\mathbb{T}^K$. Similarly, condition (3.10) needs to hold for all $\tilde{\boldsymbol{\phi}}_0$ inside $\mathbb{T}^{K-1}$. Both domains, however, contain infinitely many points. Hence, a numerical verification procedure of definition 3.2, respectively, definition 3.8, is not complete yet.

Intuitively, one would expect that if condition (3.7) holds for some $\boldsymbol{\phi}_0$, then points in the immediate vicinity of $\boldsymbol{\phi}_0$ satisfy equation (3.7) as well. More specifically, we anticipate that if the two initial angles $\boldsymbol{\phi}_0$ and $\boldsymbol{\phi}'$ are close, then the difference between $\rho_{\max}(\tau, \boldsymbol{\phi}_0)$ and $\rho_{\max}(\tau, \boldsymbol{\phi}')$ is small. To precisely asses the robustness of $\rho_{\max}(\tau, \boldsymbol{\phi}_0)$, we measure the difference between the phases $\boldsymbol{\phi}$ and $\boldsymbol{\phi}'$ in the infinity norm, i.e.

$$|\boldsymbol{\phi} - \boldsymbol{\phi}'|_\infty := \max_{1 \le k \le K} |\phi_k - \phi_k'|. \tag{3.11}$$

Moreover, we denote the following upper bound on partial derivatives of the matrix $\mathbf{A}$

$$C_{\mathbf{A}} := \sup_{\boldsymbol{\phi} \in \mathbb{T}^K} \left\| \sum_{k=1}^{K} \frac{\partial}{\partial \phi_k} \mathbf{A}(\boldsymbol{\phi}) \right\|, \tag{3.12}$$

which is finite, since $\mathbf{A}(\boldsymbol{\phi})$ is continuously differentiable by assumption. Moreover, we introduce the function

$$\eta(T(\boldsymbol{\phi}_0), \boldsymbol{\phi}_0) := \int_0^{T(\boldsymbol{\phi}_0)} \frac{\rho_{\max}(\tau, \boldsymbol{\phi}_0)}{\rho_{\min}(\tau, \boldsymbol{\phi}_0)} \, \mathrm{d}\tau. \tag{3.13}$$

With the notation (3.12) and (3.13) we state an explicit robustness estimate of the quantity $\rho_{\max}(T(\boldsymbol{\phi}_0), \boldsymbol{\phi}_0)$ with respect to the initial angle $\boldsymbol{\phi}_0$.

Lemma 3.10 (Robustness). *For any real number a greater than one, all* $\boldsymbol{\phi}_0 \in \mathbb{T}^K$ *and all* $\boldsymbol{\phi}' \in \mathbb{T}^K$ *satisfying*

$$|\boldsymbol{\phi}_0 - \boldsymbol{\phi}'|_\infty < \frac{\ln(a)}{\eta(T(\boldsymbol{\phi}_0), \boldsymbol{\phi}_0) C_{\boldsymbol{A}}}, \tag{3.14}$$

the upper bound

$$\rho_{\max}(T(\boldsymbol{\phi}_0), \boldsymbol{\phi}') < a \rho_{\max}(T(\boldsymbol{\phi}_0), \boldsymbol{\phi}_0), \tag{3.15}$$

holds.

Proof. We obtain the above robustness estimate by applying the variation of constants formula and Gronwall's inequality (cf. Teschl [13]). The details leading to equations (3.14) and (3.15) are formulated in appendix C. ∎

Definitions 3.2 or 3.8 together with the equivalence stated in theorem 3.3 and the explicit robustness estimate stated in lemma 3.10 enables us to assess the stability of the origin of system (2.1) numerically. Due to the equivalence of asymptotic stability and the existence of a contractive cover or trap established in theorem 3.3, respectively, lemma 3.9, verifying condition (3.7) or (3.10) is sufficient to conclude about asymptotic stability. Whereas asymptotic stability needs to be checked for all initial times t_0 on the non-compact real line and also requires an infinite time horizon, conditions (3.7) and (3.10) need to hold only for finite times and the initial angles take values from the compact domain $\mathbb{T}^K$, respectively $\mathbb{T}^{K-1}$. Sampling the bounded domain dense enough and checking whether condition (3.7) is satisfied for some time τ, we accomplish the first step in our stability investigation. To complete our argument, we make use of the robustness estimate lemma 3.10 to show that we have sampled either the torus $\mathbb{T}^K$ or the trap $\mathbb{T}^{K-1}$ dense enough such that equation (3.7) or (3.10) holds for every initial angle.

4. Numerical stability investigations

In the following, we use the results of §3 to assess the stability of the origin of system (2.1). First, we describe our implemented algorithm and subsequently proceed with applying it to specific examples.

(a) Implementation

Following common practice in physics, engineering and applied mathematics (e.g. Dieci *et al.* [39], Sharma & Sinha [20]), we assume that system (2.1) can be numerically integrated with arbitrary precision.[2] Picking some initial angle $\boldsymbol{\phi}_0$, we obtain $\Pi^\tau(\boldsymbol{\phi}_0)$ by numerical integration of

$$\frac{\mathrm{d}}{\mathrm{d}\tau}\Pi^\tau(\boldsymbol{\phi}_0) = \mathbf{A}(\Omega\tau + \boldsymbol{\phi}_0)\Pi^\tau(\boldsymbol{\phi}_0) \quad \text{and} \quad \Pi^0(\boldsymbol{\phi}_0) = \mathbf{I}, \tag{4.1}$$

and monitor the quantity $\rho_{\max}(\tau, \boldsymbol{\phi}_0)$ (cf. definition (3.6)). If $\rho_{\max}(\tau, \boldsymbol{\phi}_0)$ is below one for some time instance $\tau = T(\boldsymbol{\phi}_0)$, we use the robustness estimate 3.10 to obtain a neighbourhood of the initial angle $\boldsymbol{\phi}_0$ for which condition (3.8) holds as well. Setting $\rho_{\max}(T(\boldsymbol{\phi}_0), \boldsymbol{\phi}') < 1$ in equation (3.15), we obtain from equation (3.14) the neighbourhood

$$\Delta(\boldsymbol{\phi}_0) := -\frac{\ln(\rho_{\max}(T(\boldsymbol{\phi}_0), \boldsymbol{\phi}_0))}{C_{\mathbf{A}}\eta(T(\boldsymbol{\phi}_0), \boldsymbol{\phi}_0)} \quad \text{and} \quad U(\boldsymbol{\phi}_0) := \{\boldsymbol{\phi} \in \mathbb{T}^K \,|\, |\boldsymbol{\phi} - \boldsymbol{\phi}_0|_\infty \leq \Delta(\boldsymbol{\phi}_0)\}, \tag{4.2}$$

which we sketch in figure 1*a*. The length $\Delta(\boldsymbol{\phi}_0)$ is positive, since the logarithm of $\rho_{\max}(T(\boldsymbol{\phi}_0), \boldsymbol{\phi}_0) < 1$ is negative. Selecting another initial phase $\boldsymbol{\phi}_0^1$ outside of $U(\boldsymbol{\phi}_0)$. We restart the numerical integration of equation (4.1) with the initial angle $\boldsymbol{\phi}_0^1$, monitor $\rho_{\max}(\tau, \boldsymbol{\phi}_0^1)$ and obtain the next neighbourhood $U(\boldsymbol{\phi}_0^1)$ for which condition (3.8) holds (cf. green lines in figure 1*a*).

Our goal is to increment the initial angle $\boldsymbol{\phi}_0$ of $\Pi^\tau(\boldsymbol{\phi}_0)$ appropriately such that the whole torus $\mathbb{T}^K$ is contained within neighbourhoods $U(\boldsymbol{\phi}_0^l)$, i.e. $\mathbb{T}^K \subset U(\boldsymbol{\phi}_0) \cup U(\boldsymbol{\phi}_0^1) \cdots U(\boldsymbol{\phi}_0^L)$ holds. Then, we have successfully established that the origin of equation (2.1) has a contractive cover. Thus, by the virtue of theorem 3.3 the origin of system (2.1) is asymptotically stable.

The same line of reasoning holds for verifying that the origin of condition (2.1) has a contractive trap. The only difference is that a $K-1$-dimensional torus $\mathbb{T}^{K-1}$ needs to be contained with neighbourhoods $U(\boldsymbol{\phi}_0^l)$. This dimension reduction reduces the computational burden to verify definition 3.8 compared to verification of definition 3.2. Thus, our algorithm aims to numerically verify definition 3.8. However, it can be easily modified to verify definition 3.2.

[2]This assumption can be relaxed, by deriving an upper bound on the integration error, which depends on the numerical integrator used. The integration error for finite time, however, can generally be made arbitrarily small by choosing an appropriate solver with a small enough stepsize.

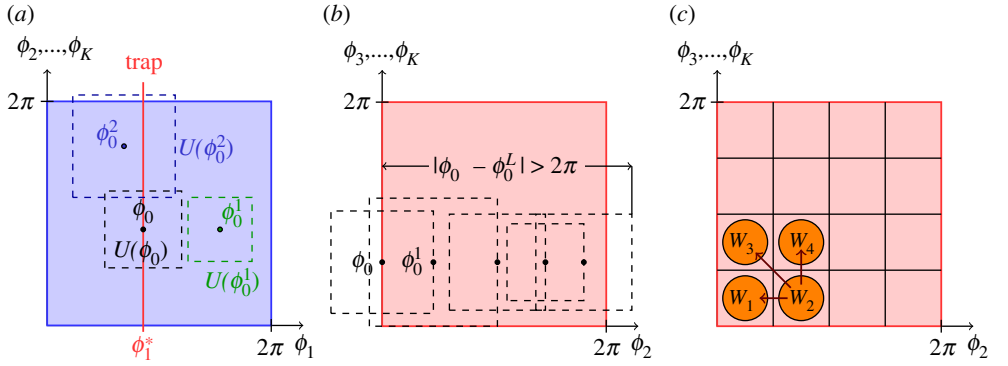

Figure 1. Sketches illustrating the numerical stability investigations of the origin of system (2.1). (*a*) Initial angles $\boldsymbol{\phi}_0^j$, their neighbourhoods $U(\boldsymbol{\phi}_0^j)$ and the $K-1$ dimensional trap for definition 3.8. (*b*) Neighbourhoods $U(\boldsymbol{\phi}_0^j)$ covering a strip of $K-1$-dimensional trap. (*c*) Segmented trap. Each segment is handed to a single worker W_j. If an individual worker (here W_2) reaches a termination condition, it sends a termination signal to the other workers. (Online version in colour.)

Various strategies can be adopted to cover the trap with neighbourhoods $U(\boldsymbol{\phi}_0^l)$. We illustrate our implemented choice in figure 1*b*. After obtaining $\Delta(\boldsymbol{\phi}_0)$, we start to integrate equation (4.1) with the initial angle $\boldsymbol{\phi}_0^1 = \boldsymbol{\phi}_0 + [\phi_1^*, \Delta(\boldsymbol{\phi}_0), 0, \ldots, 0]$ and obtain the neighbourhood $U(\boldsymbol{\phi}_0^1)$. We continue to increment the second phase until the distance between $\boldsymbol{\phi}_0$ and $\boldsymbol{\phi}_0^L$ is greater than 2π. In the case of two incommensurate frequencies in equation (2.1) ($K=2$), we have verified that definition 3.8 holds for the origin of system (2.1). For more than two incommensurate frequencies ($K>2$), we increment the third phase by the minimal distance $\Delta_{\min} := \min_{0\le l\le L}(\Delta(\boldsymbol{\phi}_0^l))$ and restart the process of assembling neighbourhoods from $[\phi_1^*, 0, \Delta_{\min}, \ldots, 0]$. We repeat this process until the third phase exceeds 2π. Analogously, we proceed for higher dimensional traps. If the last phase exceeds 2π, then we have assembled a contractive trap of the origin of system (2.1).

During our numerical verification of condition (3.10) the calculations can be terminated for two reasons. First, we set a maximal number of periods $N_{\max}$ for which we are willing to check if condition (3.10) is met. If for some initial angle no contraction is observed for $N \in [0, N_{\max}]$ (i.e. $\rho_{\max}(NT, \boldsymbol{\phi}_0) \ge 1$ for all $0 \le N \le N_{\max}$), we abort our calculations. Second, the volume of the estimated neighbourhood (4.2) can shrink in size resulting in an increased numerical effort. Thus, we truncate our calculations, if we observe that $\Delta(\boldsymbol{\phi}_0)$ shrinks below a tolerance. We emphasize that the equivalence stated in theorem 3.3 guarantees that if the origin of system (2.1) is asymptotically stable, equation (3.10) is necessarily satisfied for some time $\tau = NT$. Thus, it is only a matter of computational resources to reduce the number of asymptotically stable quasi-periodic orbits for which our algorithm is inconclusive (false negatives) to zero.

Modern high-speed computational clusters achieve their impressive performance by executing tasks in parallel. The calculations necessary to numerically check condition (3.10) are easily parallelizable. To this end, we divide the $K-1$-dimensional torus $\mathbb{T}^{K-1}$ into individual volumes V_j. Then, each V_j is assigned to a single worker, which checks if for all angles inside V_j condition (3.11) holds (cf. figure 1*c*). This task is achieved analogously as covering the whole trap $\mathbb{T}^{K-1}$ with neighbourhoods $U(\boldsymbol{\phi}_0^l)$, with the difference that only the small subset V_j of the trap needs to be contained within the union of the neighbourhoods $U(\boldsymbol{\phi}_0^l)$. If this task is successfully achieved for each V_j individually, then the origin of system (2.1) is asymptotically stable.

To increase the efficiency further and enable parameter studies, we implement cross-communication between the individual workers. If one worker terminates the calculations for one of the above-specified reasons ($\Delta(\boldsymbol{\phi}_0)$ below a tolerance or no contraction observed) it sends a termination signal to the other workers (cf. red arrows in figure 1*c*) and all computations are aborted. Thereby, we avoid that individual workers spend long computation times on their associated subset V_j although the outcome of our algorithm is doomed to be inconclusive.

We emphasize that the slow down due to cross-communication is minimal since only a single termination signal is sent.

(b) Examples

We apply our developed algorithm to assess the stability of the origin of system (2.1) to two mechanical systems. First, we consider the classic Mathieu equation, which has served as a prototype equation to demonstrate the effects of parametric excitation (cf. Nayfeh & Mook [52] or Hagedorn [53]). Subsequently, we proceed with a parametrically excited beam as a more realistic and higher dimensional engineering application. We carry out our calculations on ETH's EULER cluster with 144 computational nodes working in parallel.

(i) Mathieu equation

We consider the classical damped Mathieu equation

$$\ddot{q} + c\dot{q} + (k + k_t(t))q = 0, \tag{4.3}$$

which can describe the linearized equation of motion of a simple pendulum with moving support, the transverse vibrations of a beam with pulsating axial load or an electric circuit with a time-varying capacity (cf. Nayfeh & Mook [52] or Hagedorn [53]). As customary in structural vibrations, we include a small positive damping constant $c > 0$. Then, the origin of the Mathieu equation (4.3) without parametric excitation ($k_t(t) = 0$) is asymptotically stable. It is well known (e.g. Kovacic *et al.* [11]) that periodic parametric excitation can destabilize the trivial solution $q(t) \equiv 0$. In the following, we will consider quasi-periodic parametric excitation.

We first select $k_t(t) = 0.1(\cos(\Omega_1 t) + \cos(\Omega_2 t))$, $\Omega_2 = 1$ and $c = 0.01$ and depict the results of our stability investigations in figure 2*a*. Our QPSTAB-code ran for 4 hours to compute the data shown in figure 2*a*. The stability map looks very similar to the results of Zounes & Rand [10], who have also investigated the Mathieu equation (4.3) for this specific parametric excitation and zero damping with methods reviewed earlier. We can rigorously confirm the results of this earlier study. To illustrate trajectories for different parameter regions depicted in figure 2*a*, we numerically integrate system (4.3) from the initial condition $q_0 = 1$ and $\dot{q}_0 = 0$. For the parameters $\Omega = \sqrt{3}/3$ and $k = 0.2$, the origin of system (4.3) is stable and hence the solution decays as shown in figure 2*b*. Increasing the stiffness to $k = 0.21$, QPSTAB fails to compute a contractive trap, since no contraction is observed. This growths is shown in the bottom of figure 2*b*.

For comparison, we compute the largest Lyapunov exponent (e.g. Pikovsky & Politi [36]) for the Mathieu equation (4.3) with the parameters shown in figure 2*a*. We select $t_0 = 0$ as initial time and terminate the calculations after 2500 time units. The obtained exponent is a finite time approximation to the maximal Lyapunov exponent and hence is denoted as finite-time Lyapunov exponent (FTLE, e.g. Haller [50]). We depict its sign in figure 2*c*. Comparing figure 2*a* and 2*c*, we can conclude that the FTLE accurately identifies the stability type of the origin of system (4.3). Moreover, its computation is easier to implement and computationally less expensive than running the QPSTAB-code. As mentioned earlier, however, it is generally unclear whether the FTLE in figure 2*c* indicates the correct asymptotic trend, while QPSTAB does not suffer from this shortcoming. Thus, only after comparing figure 2*a* and 2*c* one can conclude that parameter configurations of the Mathieu equation (4.3) with an asymptotically stable origin have been accurately identified by computing the FTLE.

Based on a normal form analysis (cf. Murdock [24]) or averaging arguments (cf. Sanders *et al.* [22]), we expect the time-varying terms to effect the dynamics of system (4.3) if the forcing frequencies are resonant with the eigenfrequency $\sqrt{k}$, i.e. the following holds:

$$j_1\Omega_1 + j_2\Omega_2 + j_3\sqrt{k} = 0, \quad j_1, j_2, j_2 \in \mathbb{Z}. \tag{4.4}$$

We include resonant parameter configurations (4.4) as lines for selected integers j_i in figure 2*a*. We observe that the resonant parameter configurations of the form $k = (j_1\Omega_1 + j_2\Omega_2)^2/4$ correlate

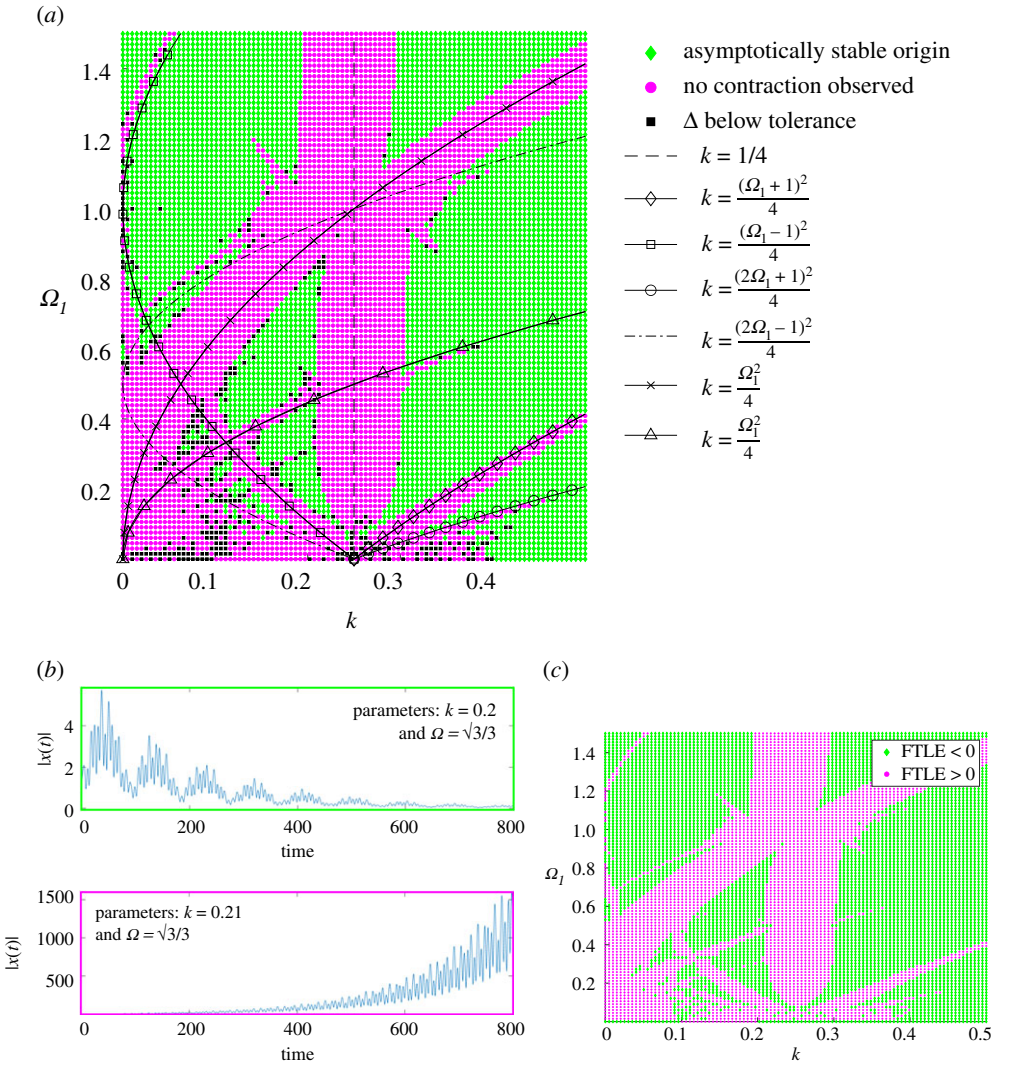

Figure 2. Stability investigations of the origin of the Mathieu equation (4.3). We select the damping $c = 0.01$ and parametric excitation $k_t(t) = 0.1(\cos(\Omega_1 t) + \cos(t))$. (*a*) Stability map indicating parameter regions for which the origin of the Mathieu equation (4.3) is asymptotically stable. (*b*) Trajectories for two different parameter configurations. (*c*) Finite time approximation of the maximal Lyapunov exponent. (Online version in colour.)

to parameter regions where our stability analysis is inconclusive. We note the similarity to instability tongues of the periodically excited Mathieu equation ($k_t(t) = \cos(\Omega t)$ in equation (4.3)), which emanate from $k = j^2\Omega^2/4$. Thus, the regions for which our analysis is inconclusive might correspond to parameter configurations for which the origin of system (4.3) is unstable. An in-depth normal form analysis or equivalently averaging could reveal such a connection rigorously. As discussed earlier, however, it is generally unclear whether the system configuration shown in figure 2*a* is within the domain of validity of such perturbation approaches.

Increasing the amplitude of the parametric excitation to $f(t) = 0.5(\cos(\Omega_1 t) + \cos(\Omega_2 t))$, and selecting the parameter values $k = 1$ and $c = 0.01$, we explore the stability of the origin of system (4.3) depending on the two forcing frequencies Ω_1 and Ω_2. We depict the results of our stability analysis in figure 3. Similarly to figure 2*a* an intricate stability map arises. Again, the influence of the time-varying terms on the dynamics of system (4.3) is clearly visible in parameter regions

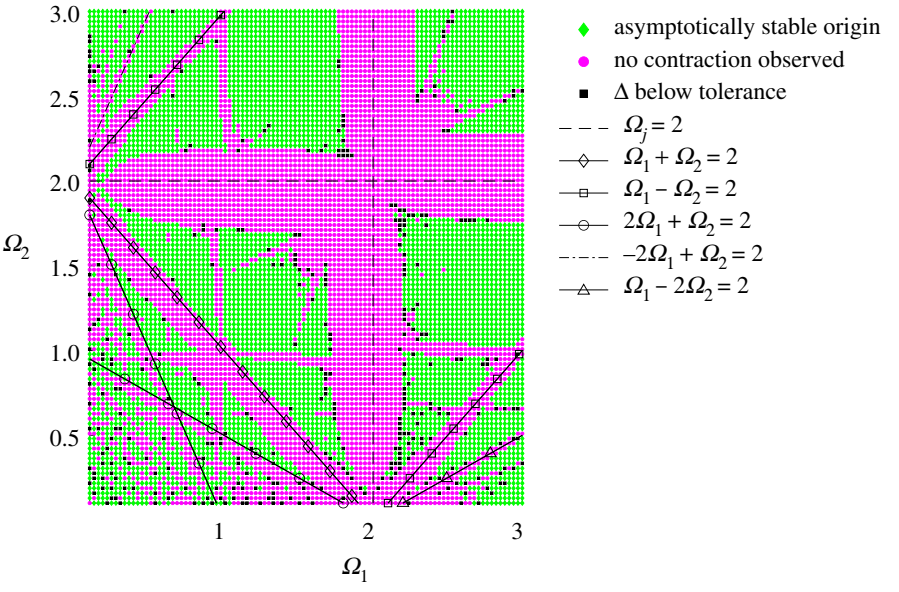

Figure 3. Stability maps indicating parameter configurations for which the origin of the Mathieu equation (4.3) is asymptotically stable. We select the parameters $k = 1$, $c = 0.01$ and $f(t) = 0.5(\cos(\Omega_1 t) + \cos(\Omega_2 t))$. (Online version in colour.)

correlating with the depicted resonant parameter configurations (4.4). We ran QPstab for about 5.5 hours to obtain the data shown in figure 3.

While most investigations on quasi-periodic orbits restrict themselves to two incommensurate frequencies, our derivations and numerical algorithm apply for any finite number of frequencies. To demonstrate this versatility, we select a parametric excitation of the Mathieu equation (4.3) containing three incommensurate frequencies $k_t(t) = 0.2(\cos(\Omega_1 t) + \cos(\Omega_2 t) + \cos(\Omega_3 t))$. Sweeping the three frequencies between 0.1 and three we obtain the three-dimensional stability map depicted on the left of figure 4. To enhance interpretation, we take two-dimensional sections of the three-dimensional stability map. Inside the first section (blue plane), the second excitation frequency is proportional to the first frequency with $\Omega_2 = \sqrt{5}/2\Omega_2$. For the second section, we choose Ω_3 to be constant and equal to $\sqrt{3}$ (red plane). We include plots indicating the stability of the origin of system (4.3) for parameter configurations inside these two sections in figure 4 whereby the frame colour distinguishes the corresponding section.

In the case of two incommensurate frequencies (cf. figures 2*a* and 3), our algorithm needs to cover a one-dimensional trap (cf. figure 1*b*). For three incommensurate frequencies illustrated in figure 4, the trap is two-dimensional, which increases the computational burden. To generate the data shown in figure 4 our QPstab script ran for about one day. Similarly to figures 2*a* and 3, we also observe in figure 4 that for parametric excitation frequencies close to two (i.e. two times the natural frequency) the time-varying terms influence the dynamics of system (4.3).

(ii) Slender beam with a moving end

As an application to a higher-dimensional system, we investigate a slender clamped-clamped beam with a moving boundary on one end prescribed by $u(t)$ (cf. figure 5). We assume constant material and geometric properties such as moment of inertia I and cross-sectional area A. We consider the case of a small radius of gyration $r = \sqrt{I/A} \ll 1$ and a small movement of the boundary $\max|u(t)|/r \ll 1$. For such beams, Nayfeh & Mook [52] derive the following partial

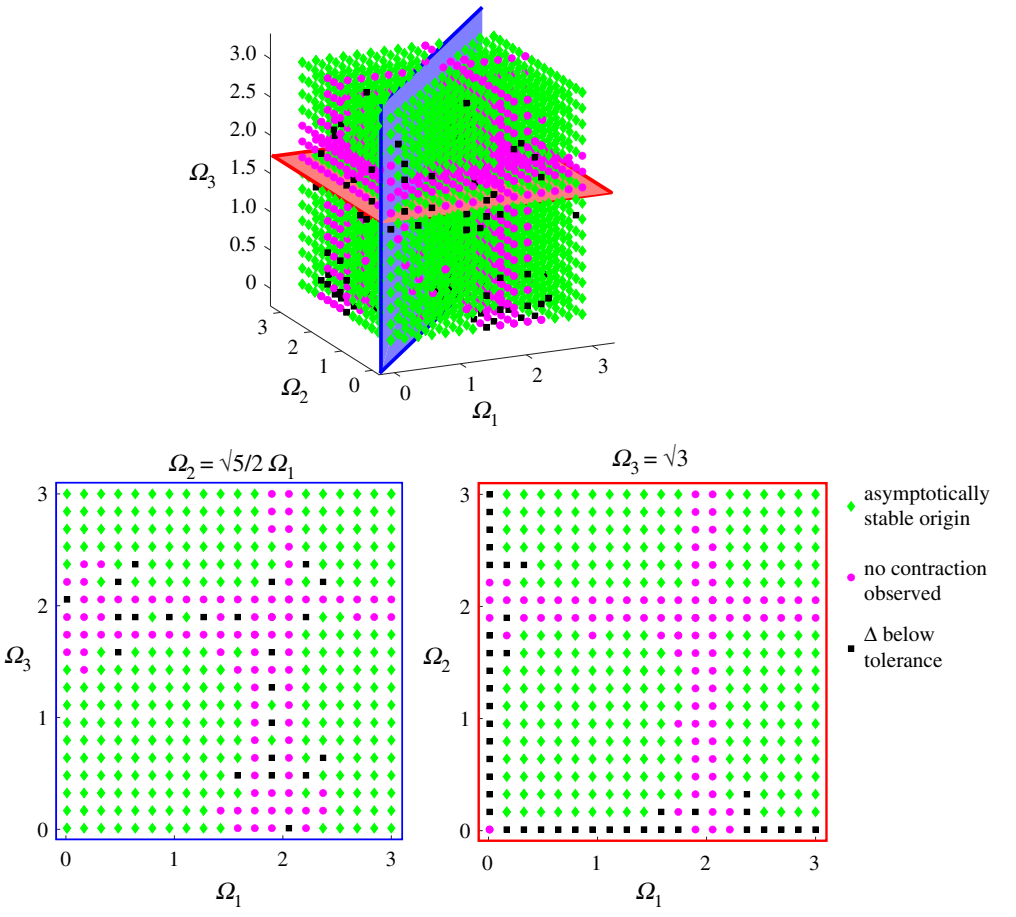

Figure 4. Stability maps indicating parameter regions for which the origin of the Mathieu equation (4.3) is asymptotically stable. We select the parameters $k = 1$, $c = 0.01$ and parametric excitation with three incommensurate frequencies $k_t(t) = 0.2(\cos(\Omega_1 t) + \cos(\Omega_2 t) + \cos(\Omega_3 t))$. We sweep the three excitation frequencies and depict the three-dimensional stability map (left). Additionally, we take two sections (blue and red) of the three-dimensional parameter space and depict the two-dimensional stability maps (middle and right). (Online version in colour.)

differential equation:

$$\left.\begin{aligned} & r^2(w_{tt} + 2\mu w_t + w_{xxxx}) - \left(u(t) + \frac{1}{2L}\int_0^L w_x^2 dx\right) w_{xx} = 0 \\ \text{and} \qquad & w(0) = w_x(0) = w(L) = w_x(L) = 0, \end{aligned}\right\} \tag{4.5}$$

governing the vertical displacement $w(x,t)$ as a function of the non-dimensional horizontal position x and the non-dimensional time t (cf. figure 5). The subscripts of w in equation (4.5) refer to partial derivative with respect to time t or space x and the constant μ is a damping parameter. To arrive at equation (4.5) Nayfeh & Mook [52] use the Euler–Bernoulli hypothesis (i.e. plane cross sections initially perpendicular to the neutral axis remain plane and perpendicular to the neutral axis after deformation), assume linear elastic material properties (Hooke's Law) and restrain themselves to a third-order approximation of the Green–Lagrange strain tensor (van Kármán strains).

We study the stability of the trivial solution $w(x,t) \equiv 0$ of system (4.5) for $u(t) = a(\cos(\Omega_1 t) + \cos(\Omega_2 t))$ with incommensurate frequencies Ω_1 and Ω_2. To this end, we discretize the beam in

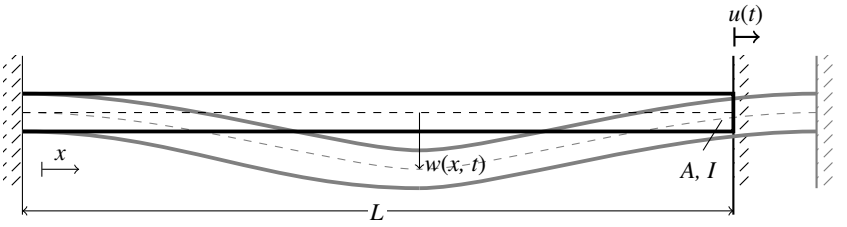

Figure 5. Clamped-clamped beam with moving end. Undeformed configuration in black and exemplary deformation in grey.

the spatial coordinate following a finite difference scheme with N equally spaced nodes x_j ($j = 1, \ldots, N$) and denote the constant distance between two neighbouring nodes by h. Then, we use the standard central finite differences

$$\left.\begin{aligned} w_{xx}(x_j) &= \frac{w(x_{j+1}) - 2w(x_j) + w(x_{j-1})}{h^2} + \mathcal{O}(h^2) \\ \text{and} \qquad w_{xxxx}(x_j) &= \frac{w(x_{j+2}) - 4w(x_{j+1}) + 6w(x_j) - 4w(x_{j-1}) + w(x_{j-2})}{h^4} + \mathcal{O}(h^2). \end{aligned}\right\} \tag{4.6}$$

To comply with the boundary conditions, we approximate the slope of w at $x = 0$ with a forward scheme $w_x(x_1) = (w(x_2) - w(x_1))/h$ and the slope at the right boundary with the backward scheme $w_x(x_N) = (w(x_N) - w(x_{N-1}))/h$. Together with requirement of zero displacement in horizontal direction at both boundaries, we obtain $w(x_1) = w(x_2) = w(x_{N-1}) = w(x_N) = 0$. Collecting the remaining degrees of freedom in the vector $\mathbf{w} := [w(x_3), w(x_4), \ldots, w(x_{N-2})]^\top \in \mathbb{R}^{N-4}$ and defining the banded matrices

$$\left.\begin{aligned} \mathbf{K} &:= \frac{1}{h^4}\begin{bmatrix} 6 & -4 & 1 & 0 & & \\ -4 & 6 & -4 & 1 & 0 & \\ 1 & -4 & 6 & -4 & 1 & 0 \\ 0 & \ddots & \ddots & \ddots & \ddots & \ddots \end{bmatrix} \\ \text{and} \qquad \mathbf{K}_t &:= \frac{1}{h^2 r^2}\begin{bmatrix} 2 & -1 & 0 & 0 & \\ -1 & 2 & -1 & 0 & \\ 0 & \ddots & \ddots & \ddots & \end{bmatrix}, \quad \mathbf{K}, \mathbf{K}_t \in \mathbb{R}^{N-4 \times N-4}, \end{aligned}\right\} \tag{4.7}$$

we obtain the discretized version of the linearization of the partial differential equation (4.5)

$$\ddot{\mathbf{w}} + 2\mu\dot{\mathbf{w}} + (\mathbf{K} + u(t)\mathbf{K}_t)\mathbf{w} = 0. \tag{4.8}$$

We select 10 nodes for the discretization $N = 10$, set the damping μ to 0.01 and the slenderness $r = 0.1$. First, we fix the length to be $L = 10$ and vary the incommensurate frequencies Ω_1 and Ω_2 between 0.1 and 3 rad s^{-1} and show the results of our stability investigations for an amplitude $a = 0.0025$ in figure 6*a*. As a second study, we fix the forcing frequencies $\Omega_1 = 1$ and $\Omega_2 = \sqrt{3}$ and vary the length of the beam and the amplitude of the parametric excitation a in figure 6*b*. QPSTAB ran for about a day to compute each stability map (figure 6*a* and 6*b*).

Figure 6 shows complex stability regions of the origin of the discretized beam (4.8). Similarly to the periodic case, the stability of the origin (4.8) is not always preserved when a parametric excitation is introduced. Contrary to the Mathieu equation (cf. figures 2*a* and 3) an explicit correlation between the regions with no contraction and resonances is not immediate in figure 6. This is due to the amount of possible resonance between the six natural frequencies and two excitation frequencies. Moreover, the natural frequencies vary with the length of the beam L in figure 6*b*. Nevertheless, our algorithm handles the beam equation (4.8) efficiently and rigorously establishes the parameter configuration for which the origin of the system (4.8) is asymptotically stable.

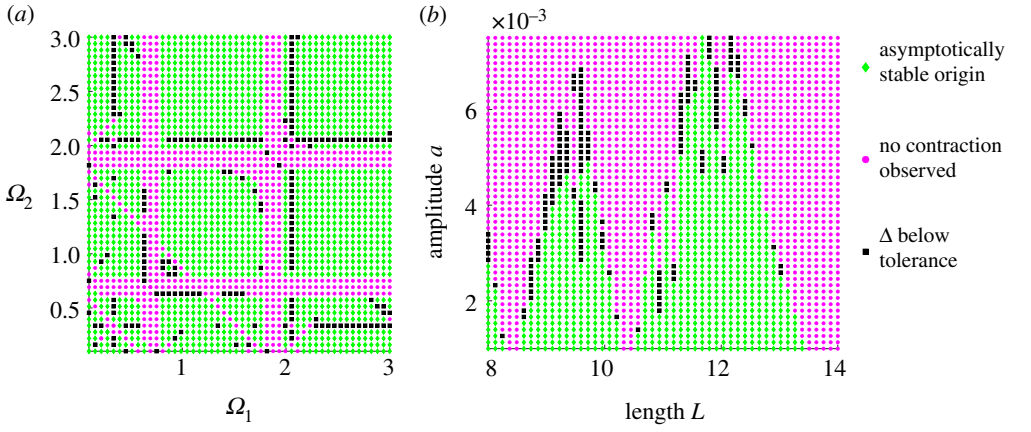

Figure 6. Stability maps indicating parameter regions for which the origin of the discretized beam (4.8) is asymptotically stable. We select 10 nodes $N = 10$, damping $\mu = 0.01$ and slenderness $r = 0.1$. (*a*) Moving end: $u(t) = 0.0025(\cos(\Omega_1 t) + \cos(\Omega_2 t))$. (*b*) Moving end: $u(t) = a(\cos(t) + \cos(\sqrt{3}t))$. (Online version in colour.)

5. Conclusion

We have presented a universal method to rigorously establish asymptotic stability of quasi-periodic orbits. Our argument relies on the repeated application of the solution map $\Pi^\tau(\boldsymbol{\phi}_0)$, which is readily available through numerical integration of the equations of variations for finite times. We introduced the notion of a contractive cover, i.e. for all initial angles there exists a time instance τ such that the map $\Pi^\tau(\boldsymbol{\phi}_0)$ is a contraction. Then, our theorem 3.3 establishes that the existence of a contractive cover is equivalent to asymptotic stability of the origin of system (2.1). Moreover, by introducing a Poincare section, we can restrict the calculations of the map $\Pi^\tau(\boldsymbol{\phi}_0)$ to a lower-dimensional contractive trap. Our robustness estimate 3.10 allows us to discretize the map $\Pi^\tau(\boldsymbol{\phi}_0)$ over the torus, whereby an observed contraction for only a finite number of initial angles can guarantee asymptotic stability of the origin of system (2.1).

Subsequently, we explicitly assemble our theoretical results in a numerical algorithm and provide QPstab, an automated MATLAB script, to assess the stability of the origin of system (2.1). We apply our algorithm to the classical Mathieu equation, whereby we rigorously confirm the results of previous studies and advance beyond available results by considering, for example, three incommensurate excitation frequencies. Finally, we proceed to a slender beam with a moving end as a more realistic engineering application and obtain stability maps for this higher dimensional system.

Despite our efforts to reduce the dimension of the sampled domain and the parallel implementation of our algorithm, the computation times can still be significant, even running QPstab on a computer cluster. An improved routine to cover the contractive trap with neighbourhoods (cf. Figure 1*b*) or an improved system-specific robustness estimate in the form of lemma 3.10 can further reduce computational times. However, we also note that already in the periodic case, calculations of the monodromy matrix can be time-consuming (cf. Peletan *et al.* [19]). Hence, customized perturbation methods such as Breunung *et al.* [54] remain important for parameter space explorations. In this setting, QPstab can verify the validity of predictions from perturbation methods.

The techniques presented can be applied to rigorously upper bound other characteristic numbers along trajectories contained in compact manifolds such as Lyapunov exponents (Chicone [51]) or generalized Lyapunov numbers (Fenichel & Moser [37]). While the notion of a contractive trap (definition 3.8) is implicitly linked to a quasi-periodic flow on the compact set (i.e. the torus), the contractive cover does not rely on such a specific flow. Hence, it is our ongoing

effort to extend our techniques and investigate the normal behaviour and Lyapunov exponents of more complex compact invariant manifolds.

In self-excited vibrations prominently modelled by the Van-der-Pol equation (e.g. Guckenheimer & Holmes [49]), a limit cycle as an invariant manifold in the phase space arises. Whereas, in system (2.1), the invariant manifold, i.e. the torus, is embedded inside an extended phase space (cf. §3). It is our goal to extend the here presented techniques to investigate the simultaneous occurrence of self-excited and externally driven vibrations.

Furthermore, it will be part of our ongoing effort to clarify the application of the presented techniques to investigate the stability of quasi-periodic linearizations of discrete dynamical systems. While a contractive cover (definition 3.2) can also be defined in the discrete setting, some additional considerations will be necessary when introducing the contractive trap (definition 3.8).

Data accessibility. QPstab, the automated MATLAB script for stability investigations of quasi-periodic orbits, as well as the data computed during this study, are publicly available at https://github.com/tbreunung/QPstab.

Competing interests. I declare I have no competing interests.

Funding. No funding has been received for this article.

Appendix A. Proof of theorem 3.3

To prove theorem 3.3, we recall the classic definition of asymptotic stability for the origin of system (2.1) (e.g. Verhulst [12]). For this purpose, we denote the trajectory of system (2.1) with initial condition $\mathbf{x}_0$ at the time $t = t_0$ by $\mathbf{x}(t; t_0, \mathbf{x}_0)$.

Definition A.1 (Asymptotic stability). The origin of system (2.1) is asymptotically stable if

(C 1) For each t_0 and each $\varepsilon > 0$, there exists $\delta = \delta(t_0, \varepsilon)$ such that for all $|\mathbf{x}_0| < \delta$, we have

$$|\mathbf{x}(t; t_0, \mathbf{x}_0)| \leq \varepsilon, \quad \text{for all } t \geq t_0. \tag{A 1}$$

(C 2) For each t_0, there exists $\delta_0 = \delta_0(t_0)$ such that for all $|\mathbf{x}_0| < \delta_0$

$$\lim_{t\to\infty} |\mathbf{x}(t; t_0, \mathbf{x}_0)| = 0, \tag{A 2}$$

holds.

We start our proof of the equivalence between asymptotic stability and a contractive cover by showing that asymptotic stability implies that definition 3.2 holds. First, we observe that not all initial phase $\boldsymbol{\phi}_0 \in \mathbb{T}^K$ are on the orbit $\boldsymbol{\phi}(t) = \boldsymbol{\Omega} t$. However, the orbit $\boldsymbol{\phi}(t)$ is dense in $\mathbb{T}^K$, since the frequency base is incommensurate (e.g. Samoilenko [27]). Hence, for all $\boldsymbol{\phi}_0$, we can find some time instance $t_0(\boldsymbol{\phi}_0)$ such that the angle $\boldsymbol{\phi}' := \boldsymbol{\phi}(t_0(\phi_0)) = \boldsymbol{\Omega} t_0(\phi_0)$ is arbitrarily close to $\boldsymbol{\phi}_0$. Continuous dependence on parameter for equation (3.1) then implies,

$$|\boldsymbol{\phi}' - \boldsymbol{\phi}_0| \leq \varepsilon \quad \Rightarrow \quad |\rho_{\max}(\tau, \boldsymbol{\phi}') - \rho_{\max}(\tau, \boldsymbol{\phi}_0)| \leq \delta(\varepsilon) < 1, \tag{A 3}$$

where $\delta(\varepsilon)$ can be made arbitrarily small by selecting ε appropriately. For the constant $\rho_{\max}(\tau, \boldsymbol{\phi}')$, we have

$$\begin{aligned}\rho_{\max}(\tau, \boldsymbol{\phi}') = \max_{|\mathbf{x}_0|=1} |\Pi^\tau(\boldsymbol{\phi}')\mathbf{x}_0| &= \frac{\max_{|\mathbf{x}_0|=\delta_0} |\Pi^{t-t_0(\boldsymbol{\phi}_0)}(\boldsymbol{\phi}')\mathbf{x}_0|}{\delta_0} \\ &\leq \frac{\sup_{|\mathbf{x}_0|<\delta_0} |\mathbf{x}(t + t_0(\boldsymbol{\phi}_0); t_0(\boldsymbol{\phi}_0), \mathbf{x}_0)|}{\delta_0}, \quad \text{for all } \boldsymbol{\phi}_0 \in \mathbb{T}^K,\end{aligned} \tag{A 4}$$

where δ_0 denotes the neighbourhood from condition (C 2). Since the limit of equation (A 2) approaches zero, for all initial times $t_0(\boldsymbol{\phi}_0)$ there exists some time instance $T(\boldsymbol{\phi}_0, \varepsilon)$ such that

$$\sup_{|\mathbf{x}_0|<\delta_0} |\mathbf{x}(T(\boldsymbol{\phi}_0, \varepsilon); t_0(\boldsymbol{\phi}_0), \mathbf{x}_0)| < (1 - \delta(\varepsilon))\delta_0, \quad \forall\, \boldsymbol{\phi}_0 \in \mathbb{T}^K, \tag{A 5}$$

holds, where the constant $\delta(\varepsilon)$ defines the neighbourhood in equation (A 3). As denoted in equation (A 5) the time instance $T(\boldsymbol{\phi}_0, \varepsilon)$ generally depends on ε. Substituting the upper bound (A 5) into equation (A 4) implies

$$\rho_{\max}(T(\boldsymbol{\phi}_0), \boldsymbol{\phi}') < 1 - \delta(\varepsilon), \quad \forall\, \boldsymbol{\phi}_0 \in \mathbb{T}^K. \tag{A 6}$$

Finally, with equation (A 6) we obtain

$$\begin{aligned}\rho_{\max}(T(\boldsymbol{\phi}_0), \boldsymbol{\phi}_0) &< \rho_{\max}(T(\boldsymbol{\phi}_0), \boldsymbol{\phi}') \\ &\quad + |\rho_{\max}(T(\boldsymbol{\phi}_0), \boldsymbol{\phi}_0) - \rho_{\max}(T(\boldsymbol{\phi}_0), \boldsymbol{\phi}')| < 1, \quad \forall\, \boldsymbol{\phi}_0 \in \mathbb{T}^K,\end{aligned} \tag{A 7}$$

which proves that condition (3.7) holds. Thus, we have proven that asymptotic stability of the origin of system (2.1) implies that a contractive cover for the origin of system (2.1) exists.

For the reverse implication, we will need to bound the constants $T(\boldsymbol{\phi}_0)$ uniformly on the domain $\mathbb{T}^K$. To this end, we note that if definition 3.2 holds it is always possible to select the time instances $T(\boldsymbol{\phi}_0)$ such that condition (3.7) is satisfied and the constants $T(\boldsymbol{\phi}_0)$ and $\rho_{\max}(T(\boldsymbol{\phi}_0), \boldsymbol{\phi}_0)$ are uniformly bounded. More specifically, we have:

Proposition A.2. *Assume that definition 3.2 holds, then the time instances $T(\boldsymbol{\phi}_0)$ can be selected such that condition (3.7) holds with*

$$\left.\begin{aligned} &T_{\min} := \inf_{\boldsymbol{\phi}_0 \in \mathbb{T}^K} T(\boldsymbol{\phi}_0) > 0, \quad T_{\max} := \sup_{\boldsymbol{\phi}_0 \in \mathbb{T}^K} T(\boldsymbol{\phi}_0) < \infty \\ \text{and} \quad &\rho_m := \sup_{\boldsymbol{\phi}_0 \in \mathbb{T}^K} \rho_{\max}(T(\boldsymbol{\phi}_0), \boldsymbol{\phi}_0) < 1. \end{aligned}\right\} \tag{A 8}$$

Proof. Continuous dependence of solutions to equation (3.1) on parameters implies that if equation (3.7) is satisfied for some initial angle $\boldsymbol{\phi}_0$ and some time $T(\boldsymbol{\phi}_0)$ then condition (3.7) also holds for initial angles $\boldsymbol{\phi}'$ sufficiently close to $\boldsymbol{\phi}_0$ for the same time $T(\boldsymbol{\phi}_0)$ (cf. also equation (A 3)). Hence, for any initial angle $\boldsymbol{\phi}_0$, we obtain a neighbourhood $U(\boldsymbol{\phi}_0)$ such that

$$\rho_{\max}(T(\boldsymbol{\phi}_0), \boldsymbol{\phi}') < 1, \quad \forall \boldsymbol{\phi}' \in U(\boldsymbol{\phi}_0) \tag{A 9}$$

holds. Since $\mathbb{T}^K$ is compact, we can select a finite number of neighbourhoods $U(\boldsymbol{\phi}_l)$ such that the union of all neighbourhoods $U(\boldsymbol{\phi}_l)$ contains $\mathbb{T}^K$ ($\mathbb{T}^K \subset U(\boldsymbol{\phi}_1) \cup U(\boldsymbol{\phi}_2) \cup \cdots \cup U(\boldsymbol{\phi}_L)$ with $L < \infty$). Thus, we obtain

$$\left.\begin{aligned} &T_{\min} = \min_{1 \le l \le L} T(\boldsymbol{\phi}_l) > 0, \quad T_{\max} = \max_{1 \le l \le L} T(\boldsymbol{\phi}_l) < \infty \\ \text{and} \quad &\rho_m = \max_{1 \le l \le L} \rho_{\max}(T(\boldsymbol{\phi}_l), \boldsymbol{\phi}_l) < 1, \end{aligned}\right\} \tag{A 10}$$

which proves the claim of proposition A.2. ∎

We proceed by recursively defining the series of angles and time instances

$$\boldsymbol{\phi}_j = \boldsymbol{\Omega} T(\boldsymbol{\phi}_{j-1}) + \boldsymbol{\phi}_{j-1} \quad \text{and} \quad t_j = T(\boldsymbol{\phi}_{j-1}) + t_{j-1}, \quad j = 1, 2, \ldots, \tag{A 11}$$

for each $\boldsymbol{\phi}_0$. The angle $\boldsymbol{\phi}_j$ denotes the angle $\boldsymbol{\phi}(t) = \boldsymbol{\Omega} t$ at $t = t_j$. Owing to proposition A.2, we can always select $T(\boldsymbol{\phi}_0)$ such that condition (3.7) holds with $0 < T_{\min} < T(\boldsymbol{\phi}_0) < T_{\max} < \infty$ and $\rho_{\max}(T(\boldsymbol{\phi}_0), \boldsymbol{\phi}_0) < \rho_m < 1$. Thus, the difference between two time instances t_j and t_{j+1} is thereby upper-bounded by $T_{\max}$ and lower-bounded by $T_{\min}$. Moreover, t_j is a monotonically increasing sequence and every time $t > t_0$ is between two subsequent time instances t_j and t_{j+1}. More specifically, for all $t > t_0$ there exists some integer j such that $t_j < t < t_{j+1}$ holds, where the integer

j is lower bounded by

$$j > \frac{t}{T_{\max}} - 1. \tag{A 12}$$

With this notation, we obtain for trajectories of system (2.1)

$$\begin{aligned} |\mathbf{x}(t;t_0,\mathbf{x}_0)| &= |\Pi^{t-t_j}(\boldsymbol{\phi}_j)\Pi^{t_j-t_{j-1}}(\boldsymbol{\phi}_{j-1})\cdots\Pi^{t_1-t_0}(\boldsymbol{\phi}_0)\mathbf{x}_0| \\ &= \left|\Pi^{t-t_j}(\boldsymbol{\phi}_j)\prod_{l=0}^{j}\Pi^{T(\boldsymbol{\phi}_l)}(\boldsymbol{\phi}_l)\mathbf{x}_0\right|. \end{aligned} \tag{A 13}$$

For the first term of equation (A 13), we recall that the distance between t and t_j is upper-bounded by $T_{\max}$. Thus, by existence and continuous dependence on parameters of solutions to equation (3.1) for finite times and the compactness of $\mathbb{T}^K$ there exists a positive constant C_T such that

$$C(T_{\max}) := \sup_{\substack{0<t<T_{\max} \\ \boldsymbol{\phi}_0\in\mathbb{T}^K}} ||\Pi^t(\boldsymbol{\phi}_0)|| < \infty, \tag{A 14}$$

holds. Using the upper bound (A 14), the lower bound (A 12) and the assertion of proposition A.2, we derive the following upper bound onto equation (A 13):

$$|\mathbf{x}(t;t_0,\mathbf{x}_0)| \leq \Big\{ C(T_{\max})|\mathbf{x}_0|, \quad \text{for } t_0 T_{\max}. \tag{A 15}$$

Thus, selecting $|\mathbf{x}_0| < \delta = \varepsilon/C_T$ ensures that equation (A 1) holds for all t_0 and $|\mathbf{x}_0| \leq \delta$, hence condition A.1 of definition A.1 is satisfied. For the limit in condition (A 2), we obtain

$$\begin{aligned} \lim_{t\to\infty}|\mathbf{x}(t;t_0,\mathbf{x}_0)| &= \lim_{t\to\infty}\left|\Pi^{t-t_j}(\boldsymbol{\phi}_j)\prod_{l=0}^{j}\Pi^{T(\boldsymbol{\phi}_l)}(\boldsymbol{\phi}_l)\mathbf{x}_0\right| \\ &\leq C(T_{\max})|\mathbf{x}_0|\lim_{t\to\infty}\rho_m^{(t/T_{\max})-1} = 0, \end{aligned} \tag{A 16}$$

where we have used the upper bound (A 15), the lower bound (A 12) and the fact that ρ_m is less than one (cf. equation (A 8)). Thus, definition 3.2 implies that the origin of system (2.1) is asymptotically stable. This completes our proof of the equivalence between a contractive cover and asymptotic stability stated in theorem 3.3.

Appendix B. Proof of lemma 3.9

We show that the existence of a contractive trap implies that a contractive cover exists and vice versa. Then, the equivalence established in theorem 3.3 implies that definition 3.8 and asymptotic stability of the origin of system (2.1) are equivalent as claimed in lemma 3.9.

We start by showing that definition 3.8 implies definition 3.2. To this end, for each $\boldsymbol{\phi}_0 \in \mathbb{T}^K$, we define the time instance τ_0 such that the first phase of $\boldsymbol{\phi}(t) = \boldsymbol{\Omega}\tau + \boldsymbol{\phi}_0$ modulo 2π is equal to ϕ_1^* ($\Omega_1\tau_0 + \phi_0^1 \mod 2\pi = \phi_1^*$). Since $\phi_1(\tau)$ has period $T = 2\pi/\Omega_1$, the time τ_0 is less than T. We denote the phase $\boldsymbol{\phi}(\tau_0) = \boldsymbol{\phi}_1$ and introduce the series of angles $\boldsymbol{\phi}_{l+1} = \boldsymbol{\Omega}N(\boldsymbol{\phi}_l)T + \boldsymbol{\phi}_l$ and time instances $\tau_{l+1} = \tau_l + N(\boldsymbol{\phi}_l)T$, whereby we obtain

$$\rho_{\max}(\tau_L,\boldsymbol{\phi}_0) = ||\Pi^{\tau_L}(\boldsymbol{\phi}_0)|| = ||\prod_{l=1}^{L}\Pi^{N(\boldsymbol{\phi}_l)T}(\boldsymbol{\phi}_l)\Pi^{\tau_0}(\boldsymbol{\phi}_0)|| \leq C(T)||\prod_{l=1}^{L}\Pi^{N(\boldsymbol{\phi}_l)T}(\boldsymbol{\phi}_l)||, \tag{B 1}$$

where the constant $C(T)$ bounds the map $\Pi^\tau(\boldsymbol{\phi}_0)$ uniformly for all $\boldsymbol{\phi}_0 \in \mathbb{T}^K$ and $0 \leq \tau \leq T$ (cf. definition (A 14)). By construction, the first phase of all $\boldsymbol{\phi}_l$ is equal to ϕ_1^*, thus the upper bound (3.11) holds. From the arguments in the proof of theorem 3.3 (i.e. Proposition A.2), we conclude $N(\phi_1^*,\tilde{\boldsymbol{\phi}})$ can be selected such that $\rho_m := \sup_{\tilde{\boldsymbol{\phi}}\in\mathbb{T}^{K-1}}||\rho_{\max}(NT,[\phi_1^*,\tilde{\boldsymbol{\phi}}])|| < 1$ and

$N_{\max} := \sup_{\tilde{\boldsymbol{\phi}} \in \mathbb{T}^{K-1}} N(\phi_1^*, \tilde{\boldsymbol{\phi}}) < \infty$ holds. With these observations, we derive the following upper bound onto equation (B 1)

$$\rho_{\max}(\tau_L, \boldsymbol{\phi}_0) = ||\Pi^{\tau_L}(\boldsymbol{\phi}_0)|| = | \leq C(T)\rho_m^L, \tag{B 2}$$

which is less than one if L is sufficiently large. The bound (B 2) implies that condition (3.7) holds and hence we have shown that condition (3.11) implies condition (3.7).

For the reverse implication, we note that limit (A 16) implies

$$\begin{aligned}\lim_{N\to\infty}(\rho_{\max}(NT, [\phi_1^*, \tilde{\boldsymbol{\phi}}])) &= \lim_{N\to\infty} ||\Pi^{NT}(\phi_1^*, \tilde{\boldsymbol{\phi}})|| \\ &= \lim_{t\to\infty} |\Pi^t(\boldsymbol{\phi}_0)\mathbf{x}_0|| = 0, \quad \forall \phi_1^* \in \mathbb{T}^1, \tilde{\boldsymbol{\phi}} \in \mathbb{T}^{K-1}\end{aligned} \tag{B 3}$$

holds. Thus for all $\phi_1^* \in \mathbb{T}^1$ and $\tilde{\boldsymbol{\phi}} \in \mathbb{T}^{K-1}$, there must be some integer N such that the norm of $\Pi^{NT}([\phi_1^*, \tilde{\boldsymbol{\phi}}])$ is less than one, i.e. condition (3.11) holds. This completes our proof of lemma 3.9.

Appendix C. Proof of the robustness estimate 3.10

We begin our proof of lemma 3.10 by rewriting the initial value problem (3.1) with the initial angle $\boldsymbol{\phi}'$ as follows:

$$\frac{\mathrm{d}}{\mathrm{d}\tau}\mathbf{x} = \mathbf{A}(\boldsymbol{\Omega}\tau + \boldsymbol{\phi}')\mathbf{x} = \mathbf{A}(\boldsymbol{\Omega}\tau + \boldsymbol{\phi}_0)\mathbf{x} + [\mathbf{A}(\boldsymbol{\Omega}\tau + \boldsymbol{\phi}') - \mathbf{A}(\boldsymbol{\Omega}\tau + \boldsymbol{\phi}_0)]\mathbf{x}. \tag{C 1}$$

By the variation of constants formula (e.g. Teschl [13]), solutions to equation (C 1) are given by

$$\mathbf{x}(T(\boldsymbol{\phi}_0)) = \Pi^{T(\boldsymbol{\phi}_0)}(\boldsymbol{\phi}_0)\mathbf{x}_0 + \Pi^{T(\boldsymbol{\phi}_0)}\int_0^{T(\boldsymbol{\phi}_0)} [\Pi^\tau(\boldsymbol{\phi}_0)]^{-1}[\mathbf{A}(\boldsymbol{\Omega}\tau + \boldsymbol{\phi}') - \mathbf{A}(\boldsymbol{\Omega}\tau + \boldsymbol{\phi}_0)]\mathbf{x}(\tau)\,\mathrm{d}\tau. \tag{C 2}$$

For the solution map $\Pi^\tau(\boldsymbol{\phi}')$, equation (C 2) implies

$$\Pi^{T(\boldsymbol{\phi}_0)}(\boldsymbol{\phi}') = \Pi^{T(\boldsymbol{\phi}_0)}(\boldsymbol{\phi}_0) + \Pi^{T(\boldsymbol{\phi}_0)}\int_0^{T(\boldsymbol{\phi}_0)} [\Pi^\tau(\boldsymbol{\phi}_0)]^{-1}[\mathbf{A}(\boldsymbol{\Omega}\tau + \boldsymbol{\phi}') - \mathbf{A}(\boldsymbol{\Omega}\tau + \boldsymbol{\phi}_0)]\Pi^\tau(\boldsymbol{\phi}')\,\mathrm{d}\tau. \tag{C 3}$$

Taking the Euclidean norm of equation (C 3), we obtain

$$\begin{aligned}\|\Pi^{T(\boldsymbol{\phi}_0)}(\boldsymbol{\phi}')\| &\leq \|\Pi^{T(\boldsymbol{\phi}_0)}(\boldsymbol{\phi}_0)\| + \|\Pi^{T(\boldsymbol{\phi}_0)}\| \\ &\quad \times \int_0^{T(\boldsymbol{\phi}_0)} \|[\Pi^\tau(\boldsymbol{\phi}_0)]^{-1}\|\,\|\mathbf{A}(\boldsymbol{\Omega}\tau + \boldsymbol{\phi}') - \mathbf{A}(\boldsymbol{\Omega}\tau + \boldsymbol{\phi}_0)\|\,\|\Pi^\tau(\boldsymbol{\phi}')\|\,\mathrm{d}\tau, \\ &\leq \rho_{\max}(T(\boldsymbol{\phi}_0), \boldsymbol{\phi}_0) + \rho_{\max}(T(\boldsymbol{\phi}_0), \boldsymbol{\phi}_0) \\ &\quad \times \int_0^{T(\boldsymbol{\phi}_0)} \frac{1}{\rho_{\min}(\tau, \boldsymbol{\phi}_0)}\,\|\mathbf{A}(\boldsymbol{\Omega}\tau + \boldsymbol{\phi}') - \mathbf{A}(\boldsymbol{\Omega}\tau + \boldsymbol{\phi}_0)\|\,\|\Pi^\tau(\boldsymbol{\phi}')\|\,\mathrm{d}\tau,\end{aligned} \tag{C 4}$$

where we have used the identities

$$||\Pi^\tau(\boldsymbol{\phi}_0)|| = \rho_{\max}(\tau, \boldsymbol{\phi}_0) \quad \text{and} \quad ||[\Pi^\tau(\boldsymbol{\phi}_0)]^{-1}|| = \frac{1}{\rho_{\min}(\tau, \boldsymbol{\phi}_0)}. \tag{C 5}$$

Dividing equation (Cï£¡ï£¡4) by $\rho_{\max}(T(\boldsymbol{\phi}_0), \boldsymbol{\phi}_0)$ and introducing the notation $u(\tau) := \rho_{\max}(\tau, \boldsymbol{\phi}')/\rho_{\max}(\tau, \boldsymbol{\phi}_0)$ we obtain

$$\begin{aligned}u(T(\boldsymbol{\phi}_0)) &\leq 1 + \int_0^{T(\boldsymbol{\phi}_0)} \frac{1}{\rho_{\min}(\tau, \boldsymbol{\phi}_0)}\|\mathbf{A}(\boldsymbol{\Omega}\tau + \boldsymbol{\phi}') - \mathbf{A}(\boldsymbol{\Omega}\tau + \boldsymbol{\phi}_0)\|\rho_{\max}(\tau, \boldsymbol{\phi}_0)\frac{\rho_{\max}(\tau, \boldsymbol{\phi}')}{\rho_{\max}(\tau, \boldsymbol{\phi}_0)}\,\mathrm{d}\tau \\ &= 1 + \int_0^{T(\boldsymbol{\phi}_0)} \frac{\rho_{\max}(\tau, \boldsymbol{\phi}_0)}{\rho_{\min}(\tau, \boldsymbol{\phi}_0)}\|\mathbf{A}(\boldsymbol{\Omega}\tau + \boldsymbol{\phi}') - \mathbf{A}(\boldsymbol{\Omega}\tau + \boldsymbol{\phi}_0)\|u(\tau)\,\mathrm{d}\tau.\end{aligned} \tag{C 6}$$

Gronwall's inequality (e.g. Teschl [13] or Verhulst [12]) applied to equation (C 6) yields

$$\rho_{\max}(T(\boldsymbol{\phi}_0), \boldsymbol{\phi}') \leq \rho_{\max}(T(\boldsymbol{\phi}_0), \boldsymbol{\phi}_0) \times \exp\left(\int_0^{T(\boldsymbol{\phi}_0)} \frac{\rho_{\max}(\tau, \boldsymbol{\phi}_0)}{\rho_{\min}(\tau, \boldsymbol{\phi}_0)} \|\mathbf{A}(\boldsymbol{\Omega}\tau + \boldsymbol{\phi}') - \mathbf{A}(\boldsymbol{\Omega}\tau + \boldsymbol{\phi}_0)\| \, \mathrm{d}\tau\right). \tag{C 7}$$

With the notation $\boldsymbol{\delta} := \boldsymbol{\phi}' - \boldsymbol{\phi}_0$ and the fundamental theorem of calculus, we obtain the upper bound

$$\begin{aligned} \|\mathbf{A}(\boldsymbol{\Omega}\tau + \boldsymbol{\phi}') - \mathbf{A}(\boldsymbol{\Omega}\tau + \boldsymbol{\phi}_0)\| &= \left\| \int_0^1 \frac{\mathrm{d}}{\mathrm{d}s} \mathbf{A}(\boldsymbol{\Omega}\tau + \boldsymbol{\phi}_0 + s\boldsymbol{\delta}) \, ds \right\| \\ &= \left\| \int_0^1 \sum_{k=1}^{K} \frac{\partial}{\partial \phi_k} (\mathbf{A}(\boldsymbol{\Omega}\tau + \boldsymbol{\phi}_0 + s\boldsymbol{\delta}))\delta_k \, \mathrm{d}s \right\| \\ &\leq \sup_{\boldsymbol{\phi} \in \mathbb{T}^K} \left\| \sum_{k=1}^{K} \frac{\partial}{\partial \phi_k} \mathbf{A}(\boldsymbol{\phi}) \right\| |\boldsymbol{\delta}|_\infty. \end{aligned} \tag{C 8}$$

With the notation (3.12), (3.13) and the upper bound (C 8), we refine the upper bound (C 7) to

$$\rho_{\max}(T(\boldsymbol{\phi}_0), \boldsymbol{\phi}') \leq \rho_{\max}(T(\boldsymbol{\phi}_0), \boldsymbol{\phi}_0) \exp[C_{\mathbf{A}} \eta(T(\boldsymbol{\phi}_0), \boldsymbol{\phi}_0) |\boldsymbol{\delta}|_\infty]. \tag{C 9}$$

Comparing equations (3.15) and (C 9) yields the condition

$$\exp(C_{\mathbf{A}} \eta(T(\boldsymbol{\phi}_0), \boldsymbol{\phi}_0) |\boldsymbol{\delta}|_\infty) < a. \tag{C 10}$$

Solving equation (C 10) for $|\boldsymbol{\delta}|_\infty = |\boldsymbol{\phi}' - \boldsymbol{\phi}_0|_\infty$ gives the neighbourhood stated in lemma 3.10.

References

1. Karavitaki KD, Mountain DC. 2007 Evidence for outer hair cell driven oscillatory fluid flow in the tunnel of corti. *Biophys. J.* **92**, 3284–3293. (doi:10.1529/biophysj.106.084087)
2. Hauck T, Schneider F. 1993 Mixed-mode and quasiperiodic oscillations in the peroxidase-oxidase reaction. *J. Phys. Chem.* **97**, 391–397. (doi:10.1021/j100104a021)
3. Oberst S, Lai J. 2011 Chaos in brake squeal noise. *J. Sound Vib.* **330**, 955–975. (doi:10.1016/j.jsv.2010.09.009)
4. Walden R, Kolodner P, Passner A, Surko C. 1984 Nonchaotic Rayleigh-Bénard convection with four and five incommensurate frequencies. *Phys. Rev. Lett.* **53**, 242. (doi:10.1103/PhysRevLett.53.242)
5. Cumming A, Linsay PS. 1988 Quasiperiodicity and chaos in a system with three competing frequencies. *Phys. Rev. Lett.* **60**, 2719. (doi:10.1103/PhysRevLett.60.2719)
6. Laskar J. 1989 A numerical experiment on the chaotic behaviour of the solar system. *Nature* **338**, 237–238. (doi:10.1038/338237a0)
7. Chua L, Ushida A. 1981 Algorithms for computing almost periodic steady-state response of nonlinear systems to multiple input frequencies. *IEEE Trans. Circuits Syst.* **28**, 953–971. (doi:10.1109/TCS.1981.1084921)
8. Dieci L, Lorenz J, Russell RD. 1991 Numerical calculation of invariant tori. *SIAM J. Sci. Stat. Comput.* **12**, 607–647. (doi:10.1137/0912033)
9. Schilder F, Osinga HM, Vogt W. 2005 Continuation of quasi-periodic invariant tori. *SIAM J. Appl. Dyn. Syst.* **4**, 459–488. (doi:10.1137/040611240)
10. Zounes RS, Rand RH. 1998 Transition curves for the quasi-periodic Mathieu equation. *SIAM J. Appl. Math.* **58**, 1094–1115. (doi:10.1137/S0036139996303877)
11. Kovacic I, Rand R, Mohamed Sah S. 2018 Mathieu's equation and its generalizations: overview of stability charts and their features. *Appl. Mech. Rev.* **70**, 020802. (doi:10.1115/1.4039144)
12. Verhulst F. 2006 *Nonlinear differential equations and dynamical systems*. Universitext. Berlin, Heidelberg: Springer.
13. Teschl G. 2012 *Ordinary differential equations and dynamical systems*, vol. 140. Providence, RI: American Mathematical Soc.

14. Johnson RA, Sell GR. 1981 Smoothness of spectral subbundles and reducibility of quasi-periodic linear differential systems. *J. Differ. Equ.* **41**, 262–288. (doi:10.1016/0022-0396(81)90062-0)
15. Jorba À, Simó C. 1992 On the reducibility of linear differential equations with quasiperiodic coefficients. *J. Differ. Equ.* **98**, 111–124. (doi:10.1016/0022-0396(92)90107-X)
16. Jorba A. 2001 Numerical computation of the normal behaviour of invariant curves of n-dimensional maps. *Nonlinearity* **14**, 943. (doi:10.1088/0951-7715/14/5/303)
17. Lazarus A, Thomas O. 2010 A harmonic-based method for computing the stability of periodic solutions of dynamical systems. *C. R. Mec.* **338**, 510–517. (doi:10.1016/j.crme.2010.07.020)
18. Krack M, Gross J. 2019 *Harmonic balance for nonlinear vibration problems*. Mathematical Engineering. Cham, Switzerland: Springer.
19. Peletan L, Baguet S, Torkhani M, Jacquet-Richardet G. 2013 A comparison of stability computational methods for periodic solution of nonlinear problems with application to rotordynamics. *Nonlinear Dyn.* **72**, 671–682. (doi:10.1007/s11071-012-0744-0)
20. Sharma A, Sinha SC. 2018 An approximate analysis of quasi-periodic systems via Floquét theory. *J. Comput. Nonlinear Dyn.* **13**, 021008. (doi:10.1115/1.4037797)
21. Guskov M, Thouverez F. 2012 Harmonic balance-based approach for quasi-periodic motions and stability analysis. *J. Vib. Acoust.* **134**, 031003. (doi:10.1115/1.4005823)
22. Sanders JA, Verhulst F, Murdock J. 2007 *Averaging methods in nonlinear dynamical systems*, vol. 59. Applied Mathematical Sciences. New York, NY: Springer.
23. Nayfeh AH. 2008 *Perturbation methods*. Wiley Classics Library Perturbation Methods. Weinheim, Germany: Wiley-VCH Verlag GmbH & Co. KGaA.
24. Murdock JA. 2006 *Normal forms and unfoldings for local dynamical systems*. Springer Monographs in Mathematics. New York, NY: Springer.
25. Belhaq M, Houssni M. 1999 Quasi-periodic oscillations, chaos and suppression of chaos in a nonlinear oscillator driven by parametric and external excitations. *Nonlinear Dyn.* **18**, 1–24. (doi:10.1023/A:1008315706651)
26. Guennoun K, Houssni M, Belhaq M. 2002 Quasi-periodic solutions and stability for a weakly damped nonlinear quasi-periodic Mathieu equation. *Nonlinear Dyn.* **27**, 211–236. (doi:10.1023/A:1014496917703)
27. Samoilenko AM. 2012 *Elements of the mathematical theory of multi-frequency oscillations*, vol. 71. Mathematics and Its Applications, Soviet Series. Dordrecht, Netherlands: Springer.
28. Haro A, de la Llave R. 2006 A parameterization method for the computation of invariant tori and their whiskers in quasi-periodic maps: rigorous results. *J. Differ. Equ.* **228**, 530–579. (doi:10.1016/j.jde.2005.10.005)
29. Oseledec VI. 1968 A multiplicative Ergodic theorem. Characteristic Ljapunov, exponents of dynamical systems. *Tr. Mosk. Mat. Obs.* **19**, 179–210.
30. Pesin YB. 1977 Characteristic Lyapunov exponents and smooth Ergodic theory. *Usp. Mat. Nauk* **32**, 55–112. (doi:10.1070/RM1977v032n04ABEH001639)
31. Benettin G, Galgani L, Giorgilli A, Strelcyn J-M. 1980 Lyapunov characteristic exponents for smooth dynamical systems and for Hamiltonian systems; a method for computing all of them. Part 1: theory. *Meccanica* **15**, 9–20. (doi:10.1007/BF02128236)
32. Benettin G, Galgani L, Giorgilli A, Strelcyn J-M. 1980 Lyapunov characteristic exponents for smooth dynamical systems and for hamiltonian systems; a method for computing all of them. Part 2: numerical application. *Meccanica (Milan)* **15**, 21–30. (doi:10.1007/BF02128237)
33. Benettin G, Galgani L, Strelcyn J-M. 1976 Kolmogorov entropy and numerical experiments. *Phys. Rev. A Gen. Phys.* **14**, 2338–2345. (doi:10.1103/PhysRevA.14.2338)
34. Wolf A, Swift JB, Swinney HL, Vastano JA. 1985 Determining Lyapunov exponents from a time series. *Physica D* **16**, 285–317. (doi:10.1016/0167-2789(85)90011-9)
35. Skokos C. 2010 The Lyapunov characteristic exponents and their computation. In *Dynamics of small solar system bodies and exoplanets*, pp. 63–135. Berlin, Germany: Springer.
36. Pikovsky A, Politi A. 2016 *Lyapunov exponents: a tool to explore complex dynamics*. Cambridge, UK: Cambridge University Press.
37. Fenichel N, Moser J. 1971 Persistence and smoothness of invariant manifolds for flows. *Ind. Univ. Math. J.* **21**, 193–226. (doi:10.1512/iumj.1972.21.21017)
38. Wiggins S. 1990 *Introduction to applied nonlinear dynamical systems and chaos*, vol. 2. Texts in Applied Mathematics. New York, NY: Springer.
39. Dieci L, Russell RD, Van Vleck ES. 1997 On the compuation of Lyapunov exponents for continuous dynamical systems. *SIAM J. Numer. Anal.* **34**, 402–423. (doi:10.1137/S0036142993247311)

40. Froeschlé C, Lega E, Gonczi R. 1997 Fast Lyapunov indicators. Application to asteroidal motion. *Celest. Mech. Dyn. Astron.* **67**, 41–62. (doi:10.1023/A:1008276418601)
41. Froeschlé C, Lega E. 2001 On the structure of symplectic mappings. The fast Lyapunov indicator: a very sensitive tool. In *New developments in the dynamics of planetary systems*, pp. 167–195. Berlin, Germany: Springer.
42. Skokos C. 2001 Alignment indices: a new, simple method for determining the ordered or chaotic nature of orbits. *J. Phys. A: Math. Gen.* **34**, 10029. (doi:10.1088/0305-4470/34/47/309)
43. Skokos C, Bountis T, Antonopoulos C. 2007 Geometrical properties of local dynamics in hamiltonian systems: the generalized alignment index (GALI) method. *Physica D* **231**, 30–54. (doi:10.1016/j.physd.2007.04.004)
44. Manos T, Bountis T, Skokos C. 2013 Interplay between chaotic and regular motion in a time-dependent barred galaxy model. *J. Phys. A: Math. Theor.* **46**, 254017. (doi:10.1088/1751-8113/46/25/254017)
45. Haller G, Sapsis T. 2010 Localized instability and attraction along invariant manifolds. *SIAM J. Appl. Dyn. Syst.* **9**, 611–633. (doi:10.1137/08074324X)
46. Kaas-Petersen C. 1985 Computation of quasi-periodic solutions of forced dissipative systems. *J. Comput. Phys.* **58**, 395–408. (doi:10.1016/0021-9991(85)90170-6)
47. Kaas-Petersen C. 1986 Computation of quasi-periodic solutions of forced dissipative systems II. *J. Comput. Phys.* **64**, 433–442. (doi:10.1016/0021-9991(86)90042-2)
48. Kaas-Petersen C. 1987 Computation, continuation, and bifurcation of torus solutions for dissipative maps and ordinary differential equations. *Physica D* **25**, 288–306. (doi:10.1016/0167-2789(87)90105-9)
49. Guckenheimer J, Holmes P. 2002 *Nonlinear oscillations, dynamical systems, and bifurcations of vector fields*, vol. **42**. Applied Mathematical Sciences. New York, NY: Springer.
50. Haller G. 2015 Lagrangian coherent structures. *Annu. Rev. Fluid Mech.* **47**, 137–162. (doi:10.1146/fluid.2015.47.issue-1)
51. Chicone C. 2006 *Ordinary differential equations with applications*, vol. 34. New York, NY: Springer Science & Business Media.
52. Nayfeh AH, Mook DT. 2008 *Nonlinear oscillations*. Physics Textbook. Weinheim: Wiley-VCH Verlag GmbH & Co. KGaA.
53. Hagedorn P. 1981 *Non-linear oscillations*. New York, NY: Oxford University Press.
54. Breunung T, Dohnal F, Pfau B. 2019 An approach to account for interfering parametric resonances and anti-resonances applied to examples from rotor dynamics. *Nonlinear Dyn.* **97**, 1837–1851. (doi:10.1007/s11071-019-04761-9)